Numerical solution to the oblique derivative boundary value problem on non-uniform grids above the Earth topography

Matej Medl'a, Karol Mikula, Róbert Čunderlík & Marek Macák

Journal of Geodesy

Continuation of Bulletin Géodésique and manuscripta geodaetica

ORIGINAL ARTICLES

A technique for routinely updating the ITU-R database using radio occultation electron density profiles
C. Brunini · F. Azpilicueta · B. Nava 813

Improvement of GPS/acoustic seafloor positioning precision through controlling the ship's track line
M. Sato · M. Fujita · Y. Matsumoto · H. Saito · T. Ishikawa · T. Asakura 825

The static gravity field model DGM-1S from GRACE and GOCE data: computation, validation and an analysis of GOCE mission's added value
H. Hashemi Farahani · P. Ditmar · R. Klees · X. Liu · Q. Zhao · J. Guo 843

IAG NEWSLETTER

IAG Newsletter
G. Tóth 869

Further articles can be found at www.springerlink.com

Indexed in *Current Contents*

Instructions for Authors for *J Geod* are available at www.springer.com/190

87 (9) 813–872 September 2013

Springer

NO SUBMISSION FEE FOR FULL COLOR ILLUSTRATIONS!

Springer

CrossMark

ORIGINAL ARTICLE

Numerical solution to the oblique derivative boundary value problem on non-uniform grids above the Earth topography

Matej Medl'a[1] · **Karol Mikula**[1,2] · **Róbert Čunderlík**[1] · **Marek Macák**[1]

Abstract The paper presents a numerical solution of the oblique derivative boundary value problem on and above the Earth's topography using the finite volume method (FVM). It introduces a novel method for constructing non-uniform hexahedron 3D grids above the Earth's surface. It is based on an evolution of a surface, which approximates the Earth's topography, by mean curvature. To obtain optimal shapes of non-uniform 3D grid, the proposed evolution is accompanied by a tangential redistribution of grid nodes. Afterwards, the Laplace equation is discretized using FVM developed for such a non-uniform grid. The oblique derivative boundary condition is treated as a stationary advection equation, and we derive a new upwind type discretization suitable for non-uniform 3D grids. The discretization of the Laplace equation together with the discretization of the oblique derivative boundary condition leads to a linear system of equations. The solution of this system gives the disturbing potential in the whole computational domain including the Earth's surface. Numerical experiments aim to show properties and demon-

strate efficiency of the developed FVM approach. The first experiments study an experimental order of convergence of the method. Then, a reconstruction of the harmonic function on the Earth's topography, which is generated from the EGM2008 or EIGEN-6C4 global geopotential model, is presented. The obtained FVM solutions show that refining of the computational grid leads to more precise results. The last experiment deals with local gravity field modelling in Slovakia using terrestrial gravity data. The GNSS-levelling test shows accuracy of the obtained local quasigeoid model.

1 Introduction

The Earth's gravity field modelling is usually formulated in terms of the geodetic boundary value problems (GBVPs). At present, a combination of terrestrial gravimetric measurements and precise 3D positioning by GNSS directly yields gravity disturbances. They naturally lead to boundary conditions (BC) of the fixed gravimetric boundary value problem (FGBVP), namely to the oblique derivative BC. Hence, from the mathematical point of view, FGBVP represents an exterior oblique derivative GBVP for the Laplace equation, cf. Koch and Pope (1972), Freeden and Kersten (1980), Bjerhammar and Svensson (1983) and Holota (1997), and many researchers have been dealing with such kind of GBVP.

Classically, a solution procedure for the oblique derivative problem has been based on integral equations using the single-layer potential, cf. Bitzadse (1968) and Miranda

✉ Matej Medl'a
medla@math.sk

Karol Mikula
mikula@math.sk

Róbert Čunderlík
cunderlik@math.sk

Marek Macák
macak@math.sk

[1] Faculty of Civil Engineering, Slovak University of Technology, Radlinského 11, 810 05 Bratislava, Slovakia

[2] Algoritmy:SK s.r.o., Sulekova 6, 81106 Bratislava, Slovakia

Springer

(1970). Koch and Pope (1972) applied such an integral equation procedure to solve the FGBVP. However, the strong nature of the singularities demanding Cauchys principal integral values turned out to be a serious obstacle (Freeden and Gerhards 2013). Later on, Freeden and Kersten (1981) proposed a new concept of approximations using the generalized Fourier expansions to transfer strongly singular integrals into regular ones. This approach based on the harmonic splines has been further developed, e.g. in Freeden (1987), Bauer (2004), Gutting (2007, 2012, 2015), see also Freeden and Michel (2004) and Freeden and Gerhards (2013).

Recently, numerical methods such as the finite element method (FEM), boundary element method (BEM) or finite volume method (FVM) have been applied to solve GBVPs. They represent an alternative to classical approaches like the spherical harmonic (SH) analysis, radial basis functions, least squares collocation or integral transforms that are standardly used for gravity field modelling. These numerical methods provide opportunities to treat the oblique derivative problem locally while considering the real Earth topography and thus to develop new approaches for gravity field modelling. Among various modelling and numerical approaches, we distinguish between solutions of GBVPs on infinite domains, see, e.g. Holota (1997), Klees et al. (2001), Nesvadba et al. (2007), Čunderlík et al. (2008) and Holota and Nesvadba (2008), and on finite domains, above the Earth's topography, either real or approximated by a sphere or an ellipsoid, cf. Fašková et al. (2010), Minarechová et al. (2015) and Macák et al. (2015).

The FEM applied to gravity field modelling has been studied in Meissl (1981), Shaofeng and Dingbo (1991) or Fašková et al. (2010). In the case of BEM, there have been published several papers; here we mention only few representative ones Klees (1995), Lehmann and Klees (1999), Klees et al. (2001), Čunderlík et al. (2008) or Čunderlík and Mikula (2010). The oblique derivative problem treated by BEM is discussed in Čunderlík et al. (2012). The first application of FVM has been introduced by Fašková (2008) and its parallel implementation by Minarechová et al. (2015). However, both papers have studied the geodetic BVP with the Neumann BC. The first insight of FVM applied to the oblique derivative BVP has been discussed in Macák et al. (2012), and this effort was further developed in Macák et al. (2015, 2016), where treatment of the oblique derivative by a central scheme and the first-order upwind schemes (LeVeque 2002), respectively, were developed for solving FGBVPs on uniform grids above the ellipsoid.

In this paper, we consider the following BVP over a local Earth topography

$$-\Delta T(\mathbf{x}) = 0, \qquad \mathbf{x} \in \Omega \subset \mathbb{R}^3, \tag{1}$$

$$v(x) \cdot \nabla T(\mathbf{x}) = g(\mathbf{x}), \quad \mathbf{x} \in \Psi \subset \partial\Omega, \tag{2}$$

$$T(\mathbf{x}) = T_{\text{Dir}}(\mathbf{x}), \quad \mathbf{x} \in \partial\Omega - \Psi, \tag{3}$$

where $T(x)$ is the disturbing potential, the vector $v(x) = \nabla U/|\nabla U|$ is a unit vector of the normal gravity, the region $\Psi \subset \partial\Omega$ represents the Earth topography, i.e. the bottom boundary, and $\partial\Omega - \Psi$ represents the top boundary together with side boundaries, see Fig. 1. In the case that the Dirichlet and oblique derivative BC are obtained from different sources, problem with a compatibility of BC can arise on the edge where bottom and side boundaries meet. In such a case, the Dirichlet BC is prescribed also in a narrow band of the bottom boundary along to this edge. Then, Ψ is given by the bottom part of $\partial\Psi$ minus the narrow band.

From the numerical point of view, we present here a new approach for solving the oblique derivative GBVP based on the FVM considered on non-uniform grids above the real Earth topography. To that goal, we develop a new method for 3D computational grid construction based on an evolving surface approach (Mikula et al. 2014). At first, we discretize the real Earth topography by a logically hexahedron grid, and then, such discretization is evolved into 3D space in order to construct a discrete 3D computational grid. The discrete surface (Earth topography) is evolved in the outer normal direction by a constant speed and by its mean curvature, and the evolution includes also a tangential component controlling a geometrical property of the 3D grid. Construction of such non-uniform 3D grid allows us to develop a new second-order discretization of the Laplace operator. Our discretization of the Laplace equation is based on the FVM, and we accompany it by a new approach for treatment of the oblique derivative given on the Earth's topography. The oblique derivative BC is under-
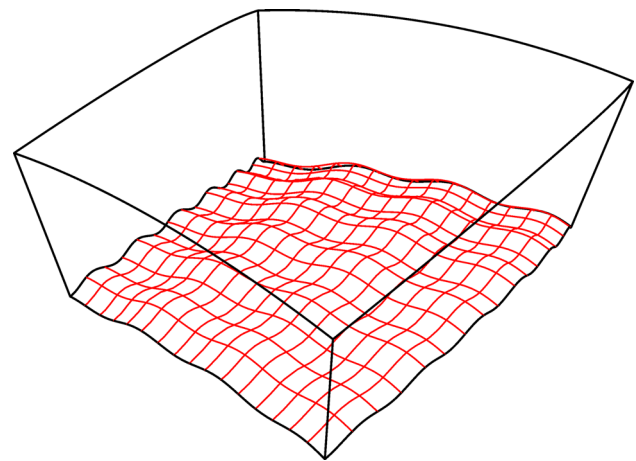
Fig. 1 Illustration of the computational domain. The *bottom red boundary* Earth's surface Ψ, the *upper boundary* ellipsoidal surface—approximation of chosen satellite orbit, the *side boundaries* borders of the local region

stood as a stationary advection equation, because from the mathematical point of view they are the same. For solving advection equations, the FVM approach is the most natural. We develop here a new upwind scheme for its treatment on non-uniform grids above the real Earth topography.

This paper is organized as follows. In Sect. 2, we introduce a method for discretization of computational domain above the Earth topography. In Sect. 3, we describe our approximation of the Laplace equation and oblique derivative BC. Finally, in Sect. 4 we present numerical experiments. The first one based on synthetic data studies an experimental order of convergence of the developed method. Next experiments show a reconstruction of the harmonic function generated by the SH-based approach at the computational domain about the extremely complicated topography in the Himalayas and in our mountainous country Slovakia. Finally, we compare efficiency of our new FVM scheme with the previous ones developed on uniform grids.

2 Construction of the computational grid above the Earth topography

Let Ω be a 3D domain bounded by a boundary $\partial\Omega$, which is composed from parts, see Fig. 1. The first part of the boundary $\partial\Omega$ represents an approximation of the Earth surface (bottom, discretized surface, in Fig. 1). The second one is given by an approximation of chosen satellite orbit at the height H (the upper ellipsoidal surface in Fig. 1). Further two boundaries are given by planes going through two meridians (front and back planar surfaces in Fig. 1), and the last two boundaries are given by planes going through two parallels (the left and the right planar surfaces in Fig. 1). Such computational domain is divided into hexahedrons by a method described as follows.

2.1 Topography evolution by mean curvature and external force

The computational domain Ω and its grid can be seen as a parametrized volume. A parametrization determines a distribution of points, which in a discrete form determines our finite volume grid. Let us denote by $S = \{\mathbf{x}(u, v, t), u \in (0, 1), v \in (0, 1), t \in (0, t_{\text{end}})\}$ the unknown parametrization of Ω. We consider that $S(u, v, 0)$ approximates the Earth's topography and we would like to force it in such a way that $S(u, v, t_{\text{end}})$ forms approximately a part of an ellipsoid at height H above the reference ellipsoid. This problem can be treated in such a way that $S(u, v, t_{\text{end}})$ will be the reference ellipsoid, which is then scaled to be approximately at the height H and $S(u, v, 0)$ remains unchanged. The 3D volume S can be seen as an evolving surface for which parameter t is the time. The grid is constructed by an evolution of the surface $S(u, v, 0)$ by its mean curvature and a force f, where f corresponds to the mean curvature of the reference ellipsoid in the point S^*. The point S^* is given by the projection of $S(u, v, t)$ to the reference ellipsoid. Using this evolution, we achieve that the surface continuously forms a shape of a part of the ellipsoid and the mathematical formulation of this process is given by Mikula et al. (2014)

$$\partial_t \mathbf{x}(u, v, t) = \varepsilon \left(k\mathbf{N} + f\mathbf{N} \right), \tag{4}$$

where unknown $\mathbf{x}$ is the position vector of the evolving surface S, k is two times its mean curvature and $\mathbf{N}$ is the normal vector at the point $\mathbf{x}$. The scalar f is the force applied in direction of the normal vector $\mathbf{N}$. The vector $k\mathbf{N}$ is computed as $k\mathbf{N} = \Delta_s \mathbf{x}$, where Δ_s is the so-called Laplace–Beltrami operator, which is the Laplace operator on a surface (Mikula et al. 2014). The scalar ε is a parameter determining how fast the surface is moving. Equation (4) is solved using the finite volume method. Boundary points of the surface do not have to be on the reference ellipsoid at time 0 due to real topography. We want them to get on the reference ellipsoid in time t_{end}. So we decided that boundary points will move linearly to the points on the ellipsoid, but we allow them also a tangential movement. Points of the grid of the computational domain Ω are discrete points of scaled S. The point are scaled around the origin $(0, 0, 0)$ with factor $1 + 240000/6378137$.

2.2 Making the uniform grid by using tangential redistribution of points

A redistribution of points on a surface is important for a uniformity of the computational grid. Another reason for a point redistribution is a numerical stability of a surface evolution. Without the redistribution of points, singularities can arise (Mikula et al. 2014). One way to achieve this goal is to maintain uniform size of finite volumes. However, in our approach we decided to maintain a uniform redistribution of chosen individual curves forming the surface (Mikula et al. 2014). These individual curves can be seen as "deformed" meridians and parallels. The discrete surface is composed by such discrete parallels and meridians which cross in discrete points $\mathbf{x}_{ij}$. In the point $\mathbf{x}_{ij}$, the i-th discrete meridian crosses the j-th discrete parallel. The uniform redistribution can be achieved by adding a tangential movement of the surface in the directions $\mathbf{T}^{p_i}$ and $\mathbf{T}^{m_j}$, where $\mathbf{T}^{p_i}$ is a tangent to the i-th parallel and $\mathbf{T}^{m_j}$ is a tangent to the j-th meridian. The tangential movement does not change the shape of a surface.

In this subsection, the tangential redistribution on individual curves is derived as in Húska et al. (2012) and Mikula et al. (2014). Let us look only on one general curve Γ on the surface. This curve can be one of the meridians or parallels,
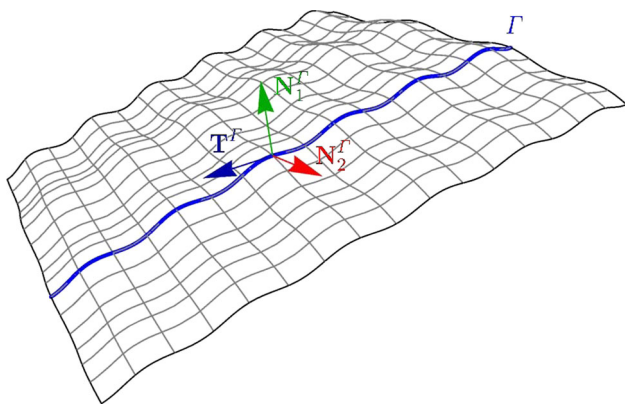
Fig. 2 Illustration of the curve Γ on the surface S and $\mathbf{T}^\Gamma, \mathbf{N}_1^\Gamma, \mathbf{N}_2^\Gamma$

and it moves as the surface S is moving. The parametrization $\Gamma = \{\mathbf{x}(u,t), u \in (0,1), t \in (0, t_{\text{end}})\}$ determines a discretization of the curve . If we have n points on a curve Γ at time point m, points of the curve are $\mathbf{x}_i = \mathbf{x}\left(\frac{i}{n}, m\right)$. If the curve has a uniform distribution at time 0, we want to preserve this distribution. If it does not have the uniform distribution, we want redistribute points uniformly. Using this parametrization, we can write $\mathbf{T}^\Gamma = \mathbf{x}_u / |\mathbf{x}_u|$.

There is another important parametrization of Γ. It is called the arc-length parametrization. We denote it by s. For this parametrization, it holds $\frac{|\mathrm{d}\mathbf{x}|}{\mathrm{d}s} = 1$. Using this parametrization, we can write $\mathbf{T}^\Gamma = \mathbf{x}_s$ and using the Frenet formula $k\mathbf{N}^\Gamma = \mathbf{T}_s^\Gamma = \mathbf{x}_{ss}$.

For better clarity in the rest of this section, we decided to denote the surface normal by $\mathbf{N}^S$ and the surface mean curvature by k^S. Movement of the curve, caused by movement of the surface by (4), is split in three perpendicular directions. The direction $\mathbf{T}^\Gamma$ is a tangent vector of the curve Γ, and other two directions $\mathbf{N}_1^\Gamma$ and $\mathbf{N}_2^\Gamma$ lie in the normal plane of the curve Γ. The direction $\mathbf{N}_1^\Gamma$ is chosen to be the normal vector of the surface $\mathbf{N}^S$. The third vector is $\mathbf{N}_2^\Gamma = \mathbf{N}_1^\Gamma \times \mathbf{T}^\Gamma$. For an illustration, see Fig. 2. In general, the curve evolution is given by the equation

$$\partial_t \mathbf{x} = U^\Gamma \mathbf{N}_1^\Gamma + V^\Gamma \mathbf{N}_2^\Gamma + A^\Gamma \mathbf{T}^\Gamma, \tag{5}$$

where $\mathbf{x}$ is the position vector of the curve Γ on the surface S. Since the curve is moving by (4), the values of U^Γ, V^Γ and A^Γ are given by

$$U^\Gamma = \left(\varepsilon\left(k^S \mathbf{N}^S + f \mathbf{N}^S\right)\right) \cdot \mathbf{N}_1^\Gamma,$$
$$V^\Gamma = \left(\varepsilon\left(k^S \mathbf{N}^S + f \mathbf{N}^S\right)\right) \cdot \mathbf{N}_2^\Gamma,$$
$$A^\Gamma = \left(\varepsilon\left(k^S \mathbf{N}^S + f \mathbf{N}^S\right)\right) \cdot \mathbf{T}^\Gamma. \tag{6}$$

Since $\mathbf{N}_1^\Gamma = \mathbf{N}^S$, $\mathbf{N}_2^\Gamma \perp \mathbf{N}^S$ and $\mathbf{T}^\Gamma \perp \mathbf{N}^S$, we have

$$U^\Gamma = \varepsilon\left(k^S + f\right),$$
$$V^\Gamma = 0,$$
$$A^\Gamma = 0. \tag{7}$$

Using this fact and by adding a new tangent velocity $\alpha^\Gamma \mathbf{T}^\Gamma$, we obtain

$$\partial_t \mathbf{x} = U^\Gamma \mathbf{N}_1^\Gamma + \alpha^\Gamma \mathbf{T}^\Gamma, \tag{8}$$

The scalar α^Γ is a quantity providing the tangential redistribution of points on the curve Γ. Since we do not want this velocity to move boundary points, we set $\alpha(0) = \alpha(1) = 0$. This quantity is derived in the rest of this subsection.

Let us introduce a function $g^\Gamma = |\mathbf{x}_u| = \sqrt{\left(\frac{\mathrm{d}x_1}{\mathrm{d}u}\right)^2 + \left(\frac{\mathrm{d}x_2}{\mathrm{d}u}\right)^2 + \left(\frac{\mathrm{d}x_3}{\mathrm{d}u}\right)^2} = \frac{\mathrm{d}s}{\mathrm{d}u}$, which can be used for the point distribution. From the discrete point of view, g^Γ is proportional to a distance between points on the curve. Let us denote by L^Γ the length of the curve Γ. If $\left(\frac{g^\Gamma}{L^\Gamma}\right)_t = 0$, the ratio of distances between points and length of the curve remains the same. This equation gives the α^Γ that preserves the initial redistribution of points.

It can be rewritten in the form

$$\left(\frac{g^\Gamma}{L^\Gamma}\right)_t = \frac{g_t^\Gamma L^\Gamma - g^\Gamma L_t^\Gamma}{\left(L^\Gamma\right)^2}, \tag{9}$$

where for g^Γ we have

$$g_t^\Gamma = |\mathbf{x}_u|_t = \frac{\mathbf{x}_u}{|\mathbf{x}_u|} \cdot (\mathbf{x}_u)_t \tag{10}$$

and

$$(\mathbf{x}_u)_t = (\mathbf{x}_t)_u = (U^\Gamma \mathbf{N}_1^\Gamma + \alpha^\Gamma \mathbf{T}^\Gamma)_u = g^\Gamma (U^\Gamma \mathbf{N}_1^\Gamma + \alpha^\Gamma \mathbf{T})_s. \tag{11}$$

From $\mathbf{T}^\Gamma = \frac{\mathbf{x}_u}{|\mathbf{x}_u|}$ and (11), we can rewrite (10) as

$$\begin{aligned}
g_t^\Gamma &= g^\Gamma \mathbf{T}^\Gamma \cdot (U^\Gamma \mathbf{N}_1^\Gamma + \alpha^\Gamma \mathbf{T})_s \\
&= g^\Gamma \mathbf{T}^\Gamma \cdot \left(U_s^\Gamma \mathbf{N}_1^\Gamma + U^\Gamma (\mathbf{N}_1^\Gamma)_s + \alpha_s^\Gamma \mathbf{T}^\Gamma + \alpha^\Gamma (\mathbf{T}^\Gamma)_s\right) \\
&= g^\Gamma \mathbf{T}^\Gamma \cdot U_s^\Gamma \mathbf{N}_1^\Gamma + g^\Gamma \mathbf{T}^\Gamma \cdot U^\Gamma (\mathbf{N}_1^\Gamma)_s \\
&\quad + g^\Gamma \mathbf{T}^\Gamma \cdot \alpha_s^\Gamma \mathbf{T}^\Gamma + g^\Gamma \mathbf{T}^\Gamma \cdot \alpha^\Gamma (\mathbf{T}^\Gamma)_s \\
&= g^\Gamma \mathbf{T}^\Gamma \cdot U^\Gamma (\mathbf{N}_1^\Gamma)_s + g^\Gamma \alpha_s^\Gamma. \tag{12}
\end{aligned}$$

Since $\mathbf{N}_1^\Gamma$ and $\mathbf{T}^\Gamma$ are perpendicular, we have

$$\mathbf{T}^\Gamma \cdot (\mathbf{N}_1^\Gamma)_s = -\mathbf{T}_s^\Gamma \cdot \mathbf{N}_1^\Gamma. \tag{13}$$

So (12) is given by

$$
\begin{aligned}
g_t^\Gamma &= -g^\Gamma U^\Gamma \mathbf{T}_s^\Gamma \cdot \mathbf{N}_1^\Gamma + g^\Gamma \alpha_s^\Gamma \\
&= -g^\Gamma U^\Gamma k^\Gamma \mathbf{N}^\Gamma \cdot \mathbf{N}_1^\Gamma + g^\Gamma \alpha_s^\Gamma
\end{aligned}
\tag{14}
$$

Let us split $k\mathbf{N}^\Gamma$ into $\mathbf{N}_1^\Gamma$ and $\mathbf{N}_2^\Gamma$

$$
k^\Gamma \mathbf{N}^\Gamma = k_1^\Gamma \mathbf{N}_1^\Gamma + k_2^\Gamma \mathbf{N}_2^\Gamma .
\tag{15}
$$

That means that k_1^Γ and k_2^Γ are given by

$$
k_1^\Gamma = k^\Gamma \mathbf{N}^\Gamma \cdot \mathbf{N}_1^\Gamma .
\tag{16}
$$

$$
k_2^\Gamma = k^\Gamma \mathbf{N}^\Gamma \cdot \mathbf{N}_2^\Gamma .
\tag{17}
$$

We can use this to rewrite (14)

$$
g_t^\Gamma = -g^\Gamma U^\Gamma k_1^\Gamma + g^\Gamma \alpha_s^\Gamma ,
\tag{18}
$$

so we have determined g_t^Γ in (9). We can determine L_t^Γ as well, by integrating Eq. (18):

$$
\begin{aligned}
L_t^\Gamma &= \int_0^1 g_t^\Gamma \, du = \int_0^1 -g^\Gamma U^\Gamma k_1^\Gamma \, du + \int_0^1 -g^\Gamma \alpha_s^\Gamma \, du \\
&= \int_\Gamma -U^\Gamma k_1^\Gamma \, ds + \alpha^\Gamma(1) - \alpha^\Gamma(0),
\end{aligned}
\tag{19}
$$

and since $\alpha^\Gamma(0) = \alpha^\Gamma(1) = 0$ we finally have

$$
L_t^\Gamma = \int_\Gamma -U^\Gamma k_1^\Gamma \, ds.
\tag{20}
$$

Let us denote

$$
\langle U^\Gamma k_1^\Gamma \rangle_\Gamma = \frac{1}{L^\Gamma} \int_\Gamma U^\Gamma k_1^\Gamma \, ds.
\tag{21}
$$

By substituting (18) and (20) into Eq. (9), we get

$$
\left(\frac{g^\Gamma}{L^\Gamma} \right)_t = \frac{g^\Gamma}{L^\Gamma} (\alpha_s^\Gamma - U^\Gamma k_1^\Gamma + \langle U^\Gamma k_1^\Gamma \rangle_\Gamma).
\tag{22}
$$

This equation determines how a distribution of points is changing in time.

If we want to determine g^Γ such that we obtain an asymptotically uniform redistribution, we can choose (Mikula and Ševčovič 2004)

$$
\left(\frac{g^\Gamma}{L^\Gamma} \right)_t = \omega \left(1 - \frac{g^\Gamma}{L^\Gamma} \right).
\tag{23}
$$

Considering (22), we see that everything in (23) is given by the evolution of the curve and the surface, except the term

α^Γ. Writing Eq. (23) in the form

$$
\alpha_s^\Gamma = -U^\Gamma k_1^\Gamma + \langle U^\Gamma k_1^\Gamma \rangle_\Gamma + \omega \left(\frac{L^\Gamma}{g^\Gamma} - 1 \right),
\tag{24}
$$

we note that we can determine α^Γ for any curve Γ on the surface S.

By adding such movement in the direction of tangent vector to the curves (in our case "deformed" meridians and parallels), the final equation for the surface evolution, which includes also tangential evolution of points, is given by

$$
\partial_t \mathbf{x} = \varepsilon (k\mathbf{N} + f\mathbf{N}) + \langle \alpha^\Gamma \mathbf{T}^\Gamma \rangle,
\tag{25}
$$

where $\langle \alpha^\Gamma \mathbf{T}^\Gamma \rangle = \sum_{\Gamma \in M^\Gamma} \alpha^\Gamma \mathbf{T}^\Gamma / |M^\Gamma|$ and M^Γ is the set of curves crossing in the point $\mathbf{x}$ which we want to redistribute and $|M^\Gamma|$ is a cardinality of the set M^Γ. Since redistributions on crossing curves do not have to be compatible, we take the average value. In the continuous case, Eqs. (25) and (4) give the same image of the evolving surface, but in the discrete case we obtain almost uniform point redistribution by using (25).

2.3 Numerical approximation of evolving surface

Let us assume that the surface is composed by n_i meridians and n_j parallels. A point of an intersection of the i-th meridian and the j-th parallel in a time index t is denoted by $\mathbf{x}_{ijt}$. Usually the time index is written as $\mathbf{x}_{ij}^t$, but in Sect. 3 we consider it as a space index, so for consistency we write it in this way. Let $p, q \in \{-1, 0, 1\}$ and let N_{int} denote a set of all (p, q), $|p| + |q| = \text{int}$, where int denote an integer number. So points $\mathbf{x}_{i+p, j+q, t}$, $(p, q) \in N_1$ are north, south, east, west neighbouring points and points $\mathbf{x}_{i+p, j+q, t}$, $(p, q) \in N_2$ are northeast, northwest, southeast, southwest neighbouring points. If we do not specify (p, q) that belongs to N_1 or N_2, we always consider that it belongs to the set N_1.

The resulting scheme for the surface evolution introduced in this subsection is semi-implicit. Some of the unknowns are taken from time $t + 1$, and others are taken from time t, so that the resulting system of equations is linear.

The surface is divided into finite volumes. A finite volume V_{ijt} is associated with the point $\mathbf{x}_{ijt}$. Note that in this subsection this is not a 3D finite volume but a 2D space finite volume in a "time" t. Vertices of the finite volume are given by centres of line segments connecting points $\mathbf{x}_{ijt}$ and $\mathbf{x}_{i+p, j+q, t}$, $(p, q) \in N_1$ and by centres of quadrilaterals given by points $\mathbf{x}_{ijt}, \mathbf{x}_{i+p, j, t}, \mathbf{x}_{i, j+q, t}, \mathbf{x}_{i+p, j+q, t}$, $(p, q) \in N_2$. These vertices are denoted by $\mathbf{x}_{ijt}^{pq}$, see Fig. 3, and they are computed by the formula
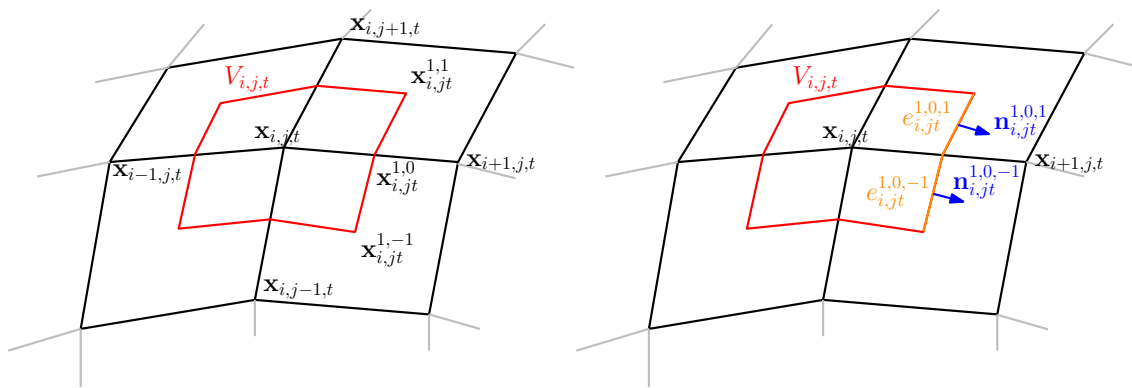
Fig. 3 *Left* finite volume with representative points and *right* finite volume with normals and edges

$$\mathbf{x}_{ijt}^{pq} = \frac{1}{4} \sum_{(l,m) \in B(p,q)} \mathbf{x}_{i+l,j+m,t}, \tag{26}$$

where $B(p,q) = \{(p,q),(p,0),(0,q),(0,0)\}$.

A boundary between V_{ijt} and $V_{i+p,j+q,t}$, $(p,q) \in N_1$ is kinked, so it is composed by two line segments. Let us denote by e_{ijt}^{pqr}, $(p,q) \in N_1, r \in \{-1,1\}$, two line segments forming the boundary between the finite volumes V_{ijt} and $V_{i+p,j+q,t}$. Let us define a function, which generate a "corner" vertex of e_{ijt}^{pqr}

$$\odot(p,q,r) = \begin{cases} (r,q), & p=0 \\ (p,r), & q=0 \end{cases} \tag{27}$$

A line segment e_{ijt}^{pqr} is then given by points $\mathbf{x}_{ijt}^{pq}$ and $\mathbf{x}_{i,j,t}^{\odot(p,q,r)}$. Let us denote $\mathbf{n}_{ijt}^{pqr}$ an outer normal to the e_{ijt}^{pqr}. For better understanding, see Fig. 3.

Let k be equal to one for simplicity. By integrating (25) over the finite volume V_{ijt}, we get

$$\int_{V_{ijt}} \partial_t \mathbf{x} \, \mathrm{d}S = \int_{V_{ijt}} \Delta_s \mathbf{x} \, \mathrm{d}S + \int_{V_{ijt}} f \mathbf{N} \, \mathrm{d}S + \int_{V_{ijt}} \langle \alpha^\Gamma \mathbf{T}^\Gamma \rangle \mathrm{d}S, \tag{28}$$

and by using Green's theorem we have

$$\int_{V_{ijt}} \partial_t \mathbf{x} \, \mathrm{d}S = \int_{\partial V_{ijt}} \nabla_s \mathbf{x} \cdot \mathbf{n}_{ijt} \, \mathrm{d}s + \int_{V_{ijt}} f \mathbf{N} \, \mathrm{d}S + \int_{V_{ijt}} \langle \alpha^\Gamma \mathbf{T}^\Gamma \rangle \mathrm{d}S. \tag{29}$$

Using definition of the finite volume, the first term on the right-hand side of (29) can be rewritten as

$$\int_{\partial V_{ijt}} \nabla_s \mathbf{x} \cdot \mathbf{n}_{ijt} \mathrm{d}s = \sum_{(p,q) \in N_1} \sum_{r \in \{-1,1\}} \int_{e_{ijt}^{pqr}} \nabla_s \mathbf{x} \cdot \mathbf{n}_{ijt}^{pqr} \mathrm{d}s$$
$$= \sum_{(p,q) \in N_1} \sum_{r \in \{-1,1\}} \int_{e_{ijt}^{pqr}} \frac{\partial \mathbf{x}}{\partial \mathbf{n}_{ijt}^{pqr}} \mathrm{d}s. \tag{30}$$

A derivative of $\mathbf{x}$ in the direction of $\mathbf{n}_{ijt}^{pqr}$ is considered constant on the boundary e_{ijt}^{pqr}. In general, a vector $\mathbf{x}_{i+p,j+q,t} - \mathbf{x}_{ijt}$ is not in the direction of the normal vector $\mathbf{n}_{ijt}^{pqr}$, so the derivative in the direction of the normal vector is approximated by a derivative in a direction of $\mathbf{x}_{i+p,j+q,t} - \mathbf{x}_{ijt}$ and a derivative in a direction of the tangent vector to e_{ijt}^{pqr}. The tangent vector to e_{ijt}^{pqr} is defined as

$$\mathbf{t}_{i,j,k}^{p,q,r} = \frac{\mathbf{x}_{i,j,k}^{\odot(p,q,r)} - \mathbf{x}_{i,j,k}^{pq}}{|\mathbf{x}_{i,j,k}^{\odot(p,q,r)} - \mathbf{x}_{i,j,k}^{pq}|}. \tag{31}$$

A unit vector $\mathbf{s}_{ijt}^{pq}$, which is pointing from the neighbouring point $\mathbf{x}_{i+p,j+q,t}$ to the point $\mathbf{x}_{i,j,t}$, is given by

$$\mathbf{s}_{ijt}^{pq} = \frac{\mathbf{x}_{i+p,j+q,t} - \mathbf{x}_{i,j,t}}{|\mathbf{x}_{i+p,j+q,t} - \mathbf{x}_{i,j,t}|}. \tag{32}$$

An approximation of the normal vector to e_{ijt}^{pqr} is defined as

$$\mathbf{n}_{ijt}^{pqr} = \frac{\mathbf{s}_{ijt}^{pq} \times \mathbf{t}_{i,j,k}^{p,q,r}}{|\mathbf{s}_{ijt}^{pq} \times \mathbf{t}_{i,j,k}^{p,q,r}|} \times \mathbf{t}_{i,j,k}^{p,q,r} \tag{33}$$

Since vectors $\mathbf{s}_{ijt}^{pq}, \mathbf{n}_{ijt}^{pqr}$ and $\mathbf{t}_{ijt}^{pqr}$ lie in the same plane, the vector $\mathbf{s}_{ijt}^{pq}$ can be expressed as a linear combination of $\mathbf{n}_{ijt}^{pqr}$, $\mathbf{t}_{ijt}^{pqr}$ and it holds

$$\nabla_s \mathbf{x} \cdot \mathbf{s}_{ijt}^{pqr} = \nabla_s \mathbf{x} \cdot (\beta_{ijt}^{pqr} \mathbf{n}_{ijt}^{pqr} + \gamma_{ijt}^{pqr} \mathbf{t}_{ijt}^{pqr})$$
$$= \beta_{ijt}^{pqr} \nabla_s \mathbf{x} \cdot \mathbf{n}_{ijt}^{pqr} + \gamma_{ijt}^{pqr} \nabla_s \mathbf{x} \cdot \mathbf{t}_{ijt}^{pqr}, \tag{34}$$

where $\beta_{ijt}^{pqr} = \mathbf{n}_{ijt}^{pqr} \cdot \mathbf{s}_{ijt}^{pq}$ and $\gamma_{ijt}^{pqr} = \mathbf{t}_{ijt}^{pqr} \cdot \mathbf{s}_{ijt}^{pq}$. Thus, the derivative in the normal direction can be expressed as

$$\nabla_s \mathbf{x} \cdot \mathbf{n}_{ijt}^{pqr} = \frac{1}{\beta_{ijt}^{pqr}} \nabla_s \mathbf{x} \cdot \mathbf{s}_{ijt}^{pqr} - \frac{\gamma_{ijt}^{pqr}}{\beta_{ijt}^{pqr}} \nabla_s \mathbf{x} \cdot \mathbf{t}_{ijt}^{pqr}, \qquad (35)$$

and approximated by

$$\nabla_s \mathbf{x} \cdot \mathbf{n}_{ijt}^{pqr} = \frac{1}{\beta_{ijt}^{pqr}} \frac{\mathbf{x}_{i+p,j+q,t+1} - \mathbf{x}_{i,j,t+1}}{|\mathbf{x}_{i+p,j+q,t} - \mathbf{x}_{i,j,t}|}$$
$$- \frac{\gamma_{ijt}^{pqr}}{\beta_{ijt}^{pqr}} \frac{\mathbf{x}_{i,j,t+1}^{\odot(p,q,r)} - \mathbf{x}_{i,j,t+1}^{pq}}{|\mathbf{x}_{i,j,t}^{\odot(p,q,r)} - \mathbf{x}_{i,j,t}^{pq}|}, \qquad (36)$$

Using this equation and because the length of e_{ijt1}^{pqr} is equal to

$$m(e_{ijt1}^{pqr}) = |\mathbf{x}_{i,j,t}^{\odot(p,q,r)} - \mathbf{x}_{i,j,t}^{pq}|, \qquad (37)$$

Eq. (30) can be approximated by

$$\sum_{(p,q)\in N_1} \sum_{r\in\{-1,1\}} \int_{e_{ijt}^{pqr}} \frac{\partial \mathbf{x}}{\partial \mathbf{n}_{ijt}^{pqr}} \mathrm{d}s \approx$$
$$\sum_{(p,q)\in N_1} \sum_{r\in\{-1,1\}} \left(\frac{m(e_{ijt1}^{pqr})}{\beta_{ijt}^{pqr}} \frac{\mathbf{x}_{i+p,j+q,t+1} - \mathbf{x}_{i,j,t+1}}{|\mathbf{x}_{i+p,j+q,t} - \mathbf{x}_{i,j,t}|} \right.$$
$$\left. - \frac{\gamma_{ijt}^{pqr}}{\beta_{ijt}^{pqr}} \left(\mathbf{x}_{i,j,t+1}^{\odot(p,q,r)} - \mathbf{x}_{i,j,t+1}^{pq} \right) \right). \qquad (38)$$

Because $\mathbf{x}_{i,j,t+1}^{\odot(p,q,r)}$ and $\mathbf{x}_{i,j,t+1}^{pq}$ are vertices of the finite volume computed as in (26), the equation can be rewritten

$$\sum_{(p,q)\in N_1} \sum_{r\in\{-1,1\}} \left(\frac{m(e_{ijt1}^{pqr})}{\beta_{ijt}^{pqr}} \frac{\mathbf{x}_{i+p,j+q,t+1} - \mathbf{x}_{i,j,t+1}}{|\mathbf{x}_{i+p,j+q,t} - \mathbf{x}_{i,j,t}|} \right.$$
$$- \frac{\gamma_{ijt}^{pqr}}{\beta_{ijt}^{pqr}} \left(\frac{1}{4} \sum_{(l,m)\in B(\odot(p,q,r))} \mathbf{x}_{i+l,j+m,t+1} \right.$$
$$\left. \left. - \frac{1}{4} \sum_{(l,m)\in B(p,q)} \mathbf{x}_{i+l,j+m,t+1} \right) \right). \qquad (39)$$

A constant value of $f\mathbf{N}_{ijt}$ is considered on the finite volume V_{ijt}. So the second term on the right-hand side of Eq. (29) can be rewritten as

$$\int_{V_{ijt}} f\mathbf{N}\mathrm{d}S = m(V_{ijt}) f\mathbf{N}_{ijt}, \qquad (40)$$

where $m(V_{ijt})$ is a 2D measure of V_{ijt}. In order to compute $\mathbf{N}_{ijt}$, we consider a vector $k\mathbf{N}_{ijt}$ computed by Eq. (39), where

all values are taken at time index t. Then, the normal vector to the surface is given by

$$\mathbf{N}_{ijt} = \frac{k\mathbf{N}_{ijt}}{|k\mathbf{N}_{ijt}|}. \qquad (41)$$

The meridians and parallels are curves according to which we are going to redistribute points on the surface. Only one meridian and one parallel go through the point $\mathbf{x}_{ijt}$. Let us consider the i-th meridian and the j-th parallel. The point $\mathbf{x}_{ijt}$ is the i-th point on the j-th parallel and the j-th point on the i-th parallel in time t. So we can write

$$\int_{V_{ijt}} \langle \alpha^\Gamma \mathbf{T}^\Gamma \rangle \mathrm{d}S = \int_{V_{ijt}} \left(\alpha^i \mathbf{T}^i + \alpha^j \mathbf{T}^j \right) /2\mathrm{d}S, \qquad (42)$$

where $\mathbf{T}^i$ ($\mathbf{T}^j$) is the tangent vector to the i-th meridian (j-th parallel). Values of $\alpha^i \mathbf{T}^i$ and $\alpha^j \mathbf{T}^j$ are considered constant on V_{ijt}, and we approximate them using central differences

$$\int_{V_{ijt}} \left(\alpha^i \mathbf{T}^i + \alpha^j \mathbf{T}^j \right) /2\mathrm{d}S =$$
$$m(V_{ijt}) \left(\alpha_{jt}^i \frac{\mathbf{x}_{i,j+1,t+1} - \mathbf{x}_{i,j-1,t+1}}{|\mathbf{x}_{i,j+1,t} - \mathbf{x}_{i,j-1,t}|} \right.$$
$$\left. + \alpha_{it}^j \frac{\mathbf{x}_{i+1,j,t+1} - \mathbf{x}_{i-1,j,t+1}}{|\mathbf{x}_{i,j+1,t} - \mathbf{x}_{i,j-1,t}|} \right) /2, \qquad (43)$$

where α_{jt}^i (α_{it}^j) is α^i (α^j) in the j-th (i-th) point on the i-th (j-th) parallel in time t. A time derivative is considered constant on the finite volume and is approximated by a finite difference

$$\int_{V_{ijt}} \partial_t \mathbf{x}\mathrm{d}S = m(V_{ijt}) \left(\frac{\mathbf{x}_{i,j,t+1} - \mathbf{x}_{ijt}}{\Delta t} \right). \qquad (44)$$

Using Eqs. (38), (40), (43) and (44), we get

$$m(V_{ijt}) \left(\frac{\mathbf{x}_{i,j,t+1} - \mathbf{x}_{ijt}}{\Delta t} \right) =$$
$$\sum_{(p,q)\in N_1} \sum_{r\in\{-1,1\}} \left(\frac{m(e_{ijt1}^{pqr})}{\beta_{ijt}^{pqr}} \frac{\mathbf{x}_{i+p,j+q,t+1} - \mathbf{x}_{i,j,t+1}}{|\mathbf{x}_{i+p,j+q,t} - \mathbf{x}_{i,j,t}|} \right.$$
$$- \frac{\alpha_{ijt}^{pqr}}{\beta_{ijt}^{pqr}} \left(\frac{1}{4} \sum_{(l,m,)\in B(\odot(p,q,r))} \mathbf{x}_{i+l,j+m,t+1} \right.$$
$$\left. \left. - \frac{1}{4} \sum_{(l,m,)\in B(p,q)} \mathbf{x}_{i+l,j+m,t+1} \right) \right) + m(V_{ijt}) f\mathbf{N}_{ijt}$$
$$+ m(V_{ijt}) \left(\alpha_{jt}^i \frac{\mathbf{x}_{i,j+1,t+1} - \mathbf{x}_{i,j-1,t+1}}{|\mathbf{x}_{i,j+1,t} - \mathbf{x}_{i,j-1,t}|} \right.$$
$$\left. + \alpha_{it}^j \frac{\mathbf{x}_{i+1,j,t+1} - \mathbf{x}_{i-1,j,t+1}}{|\mathbf{x}_{i,j+1,t} - \mathbf{x}_{i,j-1,t}|} \right) /2. \qquad (45)$$

We have a system of $n_i \times n_j$ equations with $n_i \times n_j$ unknowns $\mathbf{x}_{ij,t+1}$, where $i = 1, \ldots, n_i$ and $j = 1, \ldots, n_j$.

Values of α^i_{jt} (α^j_{it}, respectively) are computed before the system of Eq. (45) is solved. We obtain these values by solving Eq. (24). Approximating the derivative in (24) by using the backward difference and taking the right-hand side in the discrete points, we get

$$\frac{\alpha^i_{jt} - \alpha^i_{j-1,t}}{|\mathbf{x}_{i,jt} - \mathbf{x}_{i,j-1,t}|} = (U^i_{j-1/2,t} k^i_{1,j-1/2,t} - \langle U^i_t k^i_{1t} \rangle_i$$
$$+ \omega \left(\frac{L^i_t |\mathbf{x}_{i,jt} - \mathbf{x}_{i,j-1,t}|}{n_j} - 1 \right), \tag{46}$$

where

$$k^i_{m,j-1/2,t} = \left(k^i_{m,jt} - k^i_{m,,j-1,t} \right)/2, \, m = 1, 2 \tag{47}$$

$$k^i_{m,jt} = k\mathbf{N}^i_{jt} \cdot \mathbf{N}^i_{m,jt}, \, m = 1, 2 \tag{48}$$

$$\mathbf{N}^i_{1,jt} = \mathbf{N}^i_{jt}, \tag{49}$$

$$\mathbf{N}^i_{2,jt} = \mathbf{N}^i_{1,jt} \times \mathbf{T}^i_{jt}, \tag{50}$$

$$\mathbf{T}^i_{jt} = \frac{\mathbf{x}_{i,j+1,t} - \mathbf{x}_{i,j-1,t}}{|\mathbf{x}_{i,j+1,t} - \mathbf{x}_{i,j-1,t}|}, \tag{51}$$

$$k\mathbf{N}^i_{jt} = \frac{\frac{\mathbf{x}_{i,j+1,t} - \mathbf{x}_{i,j,t}}{|\mathbf{x}_{i,j+1,t} - \mathbf{x}_{i,j,t}|} - \frac{\mathbf{x}_{i,j,t} - \mathbf{x}_{i,j-1,t}}{|\mathbf{x}_{i,j,t} - \mathbf{x}_{i,j-1,t}|}}{(|\mathbf{x}_{i,j+1,t} - \mathbf{x}_{i,j,t}| + |\mathbf{x}_{i,j,t} - \mathbf{x}_{i,j-1,t}|)/2}, \tag{52}$$

$$U^i_{j-1/2,t} = \left(U^i_{j+1,t} + U^i_{j,t} \right)/2, \tag{53}$$

$$U^i_{j,t} = (\varepsilon k\mathbf{N}_{ijt} + f\mathbf{N}_{ijt}) \cdot \mathbf{N}^i_{1,jt}, \tag{54}$$

$$\langle U^i k^i_1 \rangle_i = \frac{1}{L^i_t} \sum_{l=1}^{n_j} h_{il}(U^i_{l-1/2} k^i_{1,l-1/2}), \tag{55}$$

$$L^i_t = \sum_{i=1}^{n_j} |\mathbf{x}_{i,jt} - \mathbf{x}_{i,j-1,t}|. \tag{56}$$

From (46), (55) and (56), we get

$$\alpha^i_{jt} = \alpha^i_{j-1,t} - |\mathbf{x}_{i,jt} - \mathbf{x}_{i,j-1,t}| \left(U^i_{j-1/2,t} k^i_{1,j-1/2,t} \right)$$
$$+ |\mathbf{x}_{i,jt} - \mathbf{x}_{i,j-1,t}| \sum_{l=1}^{n_j} |\mathbf{x}_{i,lt}$$
$$- \mathbf{x}_{i,l-1,t}| \left(U^i_{l-1/2,t} k^i_{1,l-1/2,t} \right)$$
$$+ \omega \left(\frac{L^i_t}{n_j} - |\mathbf{x}_{i,jt} - \mathbf{x}_{i,j-1,t}| \right), \tag{57}$$

Because $\alpha^i_{0,t} = 0$ ($\alpha^j_{0,t} = 0$), every value of $\alpha^i_{jt}(\alpha^j_{it})$ can be computed before solving system of Eq. (44).

The system of Eq. (45) can be solved using the BiCGStab method (Sleijpen and Fokkema 1993).

3 Discretization of oblique derivative BVP for Laplace equation

3.1 Approximation of the Laplace equation

Let us have Laplace equation on a three-dimensional domain Ω with Dirichlet boundary conditions

$$-\Delta T(x) = 0, x \in \Omega \tag{58}$$
$$T(x) = T_{\text{Dir}}, \, x \in \partial\Omega. \tag{59}$$

We discretize the domain Ω by the regular hexahedron grid using the approach described in the previous section. Vertices of hexahedron are the representative points of finite volumes constructed later. Representative points are denoted by $x_{i,j,k}$. Hexahedron finite volumes are constructed around inner (those that do not lie on the boundary $\partial\Omega$) representative points. Let $p, q, r \in \{-1, 0, 1\}$ and let N_{int} denote the set of all $(p, q, r), |p| + |q| + |r| = int$. Vertices of the finite volumes are denoted by $x^{p,q,r}_{i,j,k}$, where $(p, q, r) \in N_3$, see Fig. 4. Vertex $x^{p,q,r}_{i,j,k}$ is constructed in such way that is located in the centre of eight neighbouring representative points, i.e.

$$x^{p,q,r}_{i,j,k} = \frac{1}{8} \sum_{(l,m,n) \in B(p,q,r)} x_{i+l,j+m,k+n}, \tag{60}$$
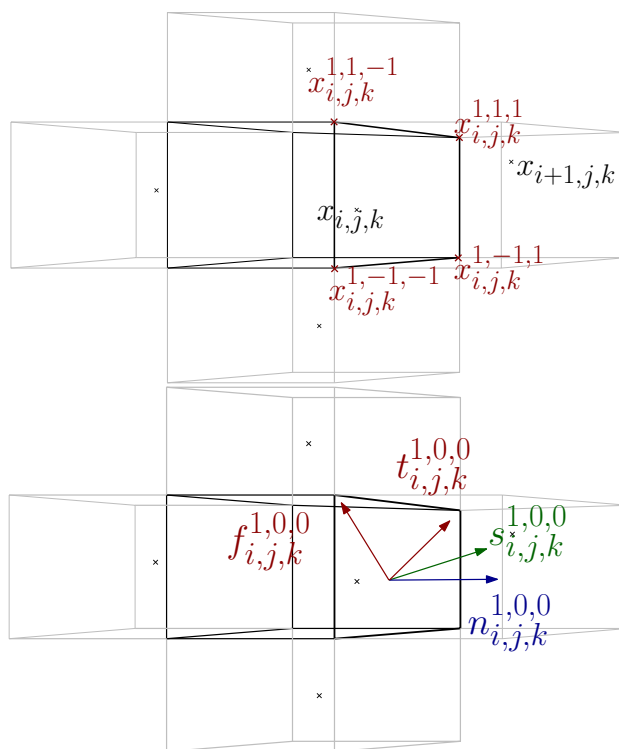

Fig. 4 Finite volume

where $B(p, q, r) = \{(p, q, r), (p, q, 0), (p, 0, r), (p, 0, 0), (0, q, r), (0, q, 0), (0, 0, r), (0, 0, 0)\}$. The finite volume associated with the representative point $x_{i,j,k}$ is denoted by $V_{i,j,k}$.

By integrating Eq. (58) over the finite volume V_{ijk}, we obtain

$$\int_{V_{i,j,k}} -\Delta T \, \mathrm{d}x = 0. \tag{61}$$

Using Green's theorem, we obtain

$$\int_{\partial V_{i,j,k}} -\nabla T \cdot \mathbf{n} \mathrm{d}\tau = 0. \tag{62}$$

Considering that the finite volume $V_{i,j,k}$ has neighbouring volumes $V_{i+p,j+q,k+r}, (p, q, r) \in N_1$ with nonzero measure of the common boundary, and $e_{i,j,k}^{p,q,r}$ is the boundary between volumes $V_{i,j,k}$ and $V_{i+p,j+q,k+r}$, we can rewrite Eq. (62) to the form

$$-\sum_{(p,q,r)\in N_1} \int_{e_{i,j,k}^{p,q,r}} \nabla T \cdot \mathbf{n} \mathrm{d}\tau = 0. \tag{63}$$

Unknown values $T_{i,j,k}$ are considered in points $x_{i,j,k}$.

Unit vector $\mathbf{s}_{i,j,k}^{p,q,r}$, which is pointing from the neighbouring point $x_{i,j,k}$ to the point $x_{i+p,j+q,k+r}$, is given by

$$\mathbf{s}_{i,j,k}^{p,q,r} = \frac{x_{i+p,j+q,k+r} - x_{i,j,k}}{|x_{i+p,j+q,k+r} - x_{i,j,k}|}, \tag{64}$$

where $|x|$ is Euclidian norm of a vector x. Let us introduce new operations on the set N_1

$$\oplus(p, q, r) = \begin{cases} (p, 1, 1), & p \neq 0 \\ (1, q, 1), & q \neq 0 \\ (1, 1, r), & r \neq 0 \end{cases},$$

$$\ominus(p, q, r) = \begin{cases} (p, -1, -1), & p \neq 0 \\ (-1, q, -1), & q \neq 0 \\ (-1, -1, r), & r \neq 0 \end{cases},$$

$$\boxplus(p, q, r) = \begin{cases} (p, 1, -1), & p \neq 0 \\ (1, q, -1), & q \neq 0 \\ (1, -1, r), & r \neq 0 \end{cases},$$

$$\boxminus(p, q, r) = \begin{cases} (p, -1, 1), & p \neq 0 \\ (-1, q, 1), & q \neq 0 \\ (-1, 1, r), & r \neq 0 \end{cases}$$

Thanks to our structure of finite volumes, the faces of finite volumes are given by four vertices. These vertices are used to compute tangent vectors. The first tangent vector $\mathbf{t}_{i,j,k}^{p,q,r}$ to the boundary between $V_{i,j,k}$ and $V_{i+p,j+q,k+r}$ is given by

$$\mathbf{t}_{i,j,k}^{p,q,r} = \frac{x_{i,j,k}^{\oplus(p,q,r)} - x_{i,j,k}^{\ominus(p,q,r)}}{|x_{i,j,k}^{\oplus(p,q,r)} - x_{i,j,k}^{\ominus(p,q,r)}|}, \tag{65}$$

where $x_{i,j,k}^{\oplus(p,q,r)}$ and $x_{i,j,k}^{\ominus(p,q,r)}$ are crosswise diagonal vertices of $e_{i,j,k}^{p,q,r}$. The second tangent vector $\mathbf{f}_{i,j,k}^{p,q,r}$ is given by other two vertices of $e_{i,j,k}^{p,q,r}$,

$$\mathbf{f}_{i,j,k}^{p,q,r} = \frac{x_{i,j,k}^{\boxplus(p,q,r)} - x_{i,j,k}^{\boxminus(p,q,r)}}{|x_{i,j,k}^{\boxplus(p,q,r)} - x_{i,j,k}^{\boxminus(p,q,r)}|}. \tag{66}$$

The normal vector to the boundary of the finite volume is then defined by

$$\mathbf{n}_{i,j,k}^{p,q,r} = \mathbf{t}_{i,j,k}^{p,q,r} \times \mathbf{f}_{i,j,k}^{p,q,r}. \tag{67}$$

where $\mathbf{n}_{i,j,k}^{p,q,r}$ is the outer normal relative to the finite volume $V_{i,j,k}$ (see Fig. 4).

Since the vector $\mathbf{s}_{ijk}^{pqr}$ can be expressed as a linear reconstruction of $\mathbf{n}_{ijk}^{pqr}, \mathbf{t}_{ijk}^{pqr}, \mathbf{f}_{ijk}^{pqr}$, it holds

$$\begin{aligned} \nabla T \cdot \mathbf{s}_{ijk}^{pqr} &= \nabla T \cdot (\beta_{ijk}^{pqr} \mathbf{n}_{ijk}^{pqr} + \alpha_{ijk}^{pqr} \mathbf{t}_{ijk}^{pqr} + \gamma_{ijk}^{pqr} \mathbf{f}_{ijk}^{pqr}) \\ &= \beta_{ijk}^{pqr} \nabla T \cdot \mathbf{n}_{ijk}^{pqr} + \alpha_{ijk}^{pqr} \nabla T \cdot \mathbf{t}_{ijk}^{pqr} + \gamma_{ijk}^{pqr} \nabla T \cdot \mathbf{f}_{ijk}^{pqr}, \end{aligned} \tag{68}$$

where coefficients $\alpha_{ijk}^{pqr}, \beta_{ijk}^{pqr}$ and γ_{ijk}^{pqr} are given by solving a linear system of equations

$$\mathbf{s}_{ijk}^{pqr} = \beta_{ijk}^{pqr} \mathbf{n}_{ijk}^{pqr} + \alpha_{ijk}^{pqr} \mathbf{t}_{ijk}^{pqr} + \gamma_{ijk}^{pqr} \mathbf{f}_{ijk}^{pqr}. \tag{69}$$

Therefore, for the derivative in the direction of normal we get

$$\nabla T \cdot \mathbf{n}_{ijk}^{pqr} = \frac{1}{\beta_{ijk}^{pqr}} (\nabla T \cdot \mathbf{s}_{ijk}^{pqr} - \alpha_{ijk}^{pqr} \nabla T \cdot \mathbf{t}_{ijk}^{pqr} - \gamma_{ijk}^{pqr} \nabla T \cdot \mathbf{f}_{ijk}^{pqr}). \tag{70}$$

Equation (70) is approximated by

$$\begin{aligned} &\frac{1}{\beta_{ijk}^{pqr}} (\nabla T \cdot \mathbf{s}_{ijk}^{pqr} - \alpha_{ijk}^{pqr} \nabla T \cdot \mathbf{t}_{ijk}^{pqr} - \gamma_{ijk}^{pqr} \nabla T \cdot \mathbf{f}_{ijk}^{pqr}) \\ &\approx \frac{1}{\beta_{ijk}^{pqr}} \frac{T_{ijk} - T_{i+p,j+q,k+r}}{d_{ijk}^{pqr}} - \frac{\alpha_{ijk}^{pqr}}{\beta_{ijk}^{pqr}} \frac{T_{i,j,k}^{\oplus(p,q,r)} - T_{i,j,k}^{\ominus(p,q,r)}}{|x_{i,j,k}^{\oplus(p,q,r)} - x_{i,j,k}^{\ominus(p,q,r)}|} \\ &\quad - \frac{\gamma_{ijk}^{pqr}}{\beta_{ijk}^{pqr}} \frac{T_{i,j,k}^{\boxplus(p,q,r)} - T_{i,j,k}^{\boxminus(p,q,r)}}{|x_{i,j,k}^{\boxplus(p,q,r)} - x_{i,j,k}^{\boxminus(p,q,r)}|}, \end{aligned} \tag{71}$$

where $T_{i,j,k}^{\oplus(p,q,r)}$ are the values at the points $x_{i,j,k}^{\oplus(p,q,r)}$ and d_{ijk}^{pqr} is the distance between $x_{i,j,k}^{p,q,r}$ and $x_{i,j,k}$.

Equation (63) can be rewritten using Eq. (71) in the form

$$
\begin{aligned}
-\sum_{(p,q,r)\in N_1} m(e_{ijk}^{pqr})\Bigg(& \frac{1}{\beta_{ijk}^{pqr}} \frac{T_{ijk} - T_{i+p,j+q,k+r}}{d_{ijk}^{pqr}} \\
& -\frac{\alpha_{ijk}^{pqr}}{\beta_{ijk}^{pqr}} \frac{T_{i,j,k}^{\oplus(p,q,r)} - T_{i,j,k}^{\ominus(p,q,r)}}{|x_{i,j,k}^{\oplus(p,q,r)} - x_{i,j,k}^{\ominus(p,q,r)}|} \\
& -\frac{\gamma_{ijk}^{pqr}}{\beta_{ijk}^{pqr}} \frac{T_{i,j,k}^{\boxplus(p,q,r)} - T_{i,j,k}^{\boxminus(p,q,r)}}{|x_{i,j,k}^{\boxplus(p,q,r)} - x_{i,j,k}^{\boxminus(p,q,r)}|}\Bigg) = 0,
\end{aligned} \tag{72}
$$

where $m(e_{ijk}^{pqr})$ is the area of the face e_{ijk}^{pqr}. For the finite volumes, that are adjacent to the boundary finite volumes, the value $T_{i+p,j+q,k+r}$ is given by the Dirichlet boundary condition (59). Values $T_{i,j,k}^{\oplus(p,q,r)}$ are not given in representative points, but in points $x_{i,j,k}^{\oplus(p,q,r)}$, which are vertices of the finite volume. They are at the centre of the corresponding representative points (60). So values $T_{i,j,k}^{\oplus(p,q,r)}$ are approximated by

$$
\begin{aligned}
T_{i,j,k}^{\oplus(p,q,r)} &= T(x_{i,j,k}^{\oplus(p,q,r)}) \\
&= \frac{1}{8}\sum_{(l,m,n)\in B(\oplus(p,q,r))} T_{i+l,j+m,k+n},
\end{aligned} \tag{73}
$$

and values $T_{i,j,k}^{\ominus(p,q,r)}$, $T_{i,j,k}^{\boxplus(p,q,r)}$, $T_{i,j,k}^{\boxminus(p,q,r)}$ in Eq. (72) can be expressed similarly.

Equation (73) is given for every inner finite volume $V_{i,j,k}$ with the unknown value $T_{i,j,k}$. Therefore, we have as many equations as unknowns, and we get the linear system, which can be solved, e.g. by BiCGStab method (Sleijpen and Fokkema 1993). A numerical experiment for solving the problem (58–59) in this way is presented in Sect. 4.

3.2 Approximation of the oblique derivative boundary condition

Let us have the Laplace equation (58) on the domain Ω with prescribed derivative in the direction v, pointing outward from Ω, on the part of the domain boundary Ψ and the Dirichlet boundary condition (59) on the rest of the boundary. The oblique derivative boundary condition is thus given by

$$
v(x) \cdot \nabla T(x) = g(x), \ x \in \Psi. \tag{74}
$$

The computational domain is divided by finite volumes as in the previous subsection. However, the finite volumes are constructed also around representative points on the boundary Ψ. Vertices common to boundary finite volumes and inner finite volumes are located at the centre of the representative points, defined by (60). Other vertices of the boundary finite

volumes are obtained by mirroring of the former ones through Ψ. The set of added finite volumes is denoted by O.

We understand Eq. (74) as advection equation, see LeVeque (2002), and we integrate it over the finite volume $V_{i,j,k} \in O$:

$$
\int_{V_{i,j,k}} v \cdot \nabla T \, dx = \int_p g \, dx. \tag{75}
$$

Since

$$
v \cdot \nabla T = \nabla \cdot (vT) - T\nabla \cdot v, \tag{76}
$$

where $\nabla \cdot = \text{div}$, we can rewrite Eq. (75) into the form

$$
\int_{V_{i,j,k}} \nabla \cdot (vT) \, dx - \int_{V_{i,j,k}} T\nabla \cdot v \, dx = \int_{V_{i,j,k}} g \, dx. \tag{77}
$$

Since T is considered constant on the finite volume, then

$$
\int_{V_{i,j,k}} \nabla \cdot (vT) \, dx - T_{i,j,k}\int_{V_{i,j,k}} \nabla \cdot v \, dx = \int_{V_{i,j,k}} g \, dx. \tag{78}
$$

Using Green's theorem, we have

$$
\int_{\partial V_{i,j,k}} Tv \cdot \mathbf{n} \, ds - T_{i,j,k}\int_{\partial V_{i,j,k}} v \cdot \mathbf{n} \, ds = \int_{V_{i,j,k}} g \, dx. \tag{79}
$$

Suppose that g is constant on the finite volume and that T is constant on the faces $e_{i,j,k}^{p,q,r}$, then Eq. (79) takes the form

$$
\begin{aligned}
&\sum_{(p,q,r)\in N_1} T_{i,j,k}^{p,q,r} \int_{e_{i,j,k}^{p,q,r}} v \cdot \mathbf{n} \, ds \\
&-T_{i,j,k}\sum_{(p,q,r)\in N_1} \int_{e_{i,j,k}^{p,q,r}} v \cdot \mathbf{n} \, ds = |V_{i,j,k}|g,
\end{aligned} \tag{80}
$$

where $T_{i,j,k}^{p,q,r}$ is the value on the boundary $e_{i,j,k}^{p,q,r}$ and $|V_{i,j,k}|$ is the volume of the finite volume $V_{i,j,k}$.

The upwind principle (LeVeque 2002) will be used in the sequel. Let us define the integrated flux over $e_{i,j,k}^{p,q,r}$ by

$$
v_{i,j,k}^{p,q,r} = \int_{e_{i,j,k}^{p,q,r}} v \cdot \mathbf{n} \, ds. \tag{81}
$$

If $v_{i,j,k}^{p,q,r} > 0$, $e_{i,j,k}^{p,q,r}$ is an outflow face. Thus, $T_{i,j,k}^{p,q,r}$ should be computed by using the information from inside of the finite volume, $T_{i,j,k}^{p,q,r} := T_{i,j,k} + \nabla T_{i,j,k} \cdot (x_{i,j,k}^{p,q,r} - x_{i,j,k})$, where $\nabla T_{i,j,k}$ is an approximation of the gradient in the finite volume $V_{i,j,k}$. If $v_{i,j,k}^{p,q,r} < 0$, $e_{i,j,k}^{p,q,r}$ represents an inflow face;
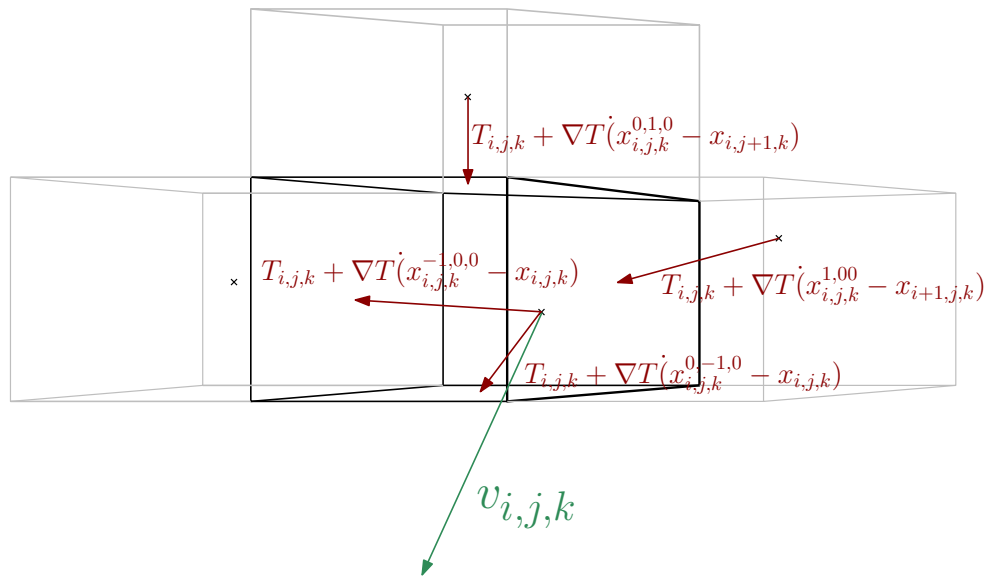
Fig. 5 Neighbouring finite volume

thus, $T_{i,j,k}^{p,q,r}$ is computed using information from the neighbouring finite volume. Hence, $T_{i,j,k}^{p,q,r} := T_{i+p,j+q,k+r} + \nabla T_{i+p,j+q,k+r} \cdot (x_{i,j,k}^{p,q,r} - x_{i+p,j+q,k+r})$, see Fig. 5.

Let us split the set N_1 for (i, j, k) into $N_1^{in}(i, j, k)$ and $N_1^{out}(i, j, k)$, where $N_1^{in}(i, j, k)$ are indexes of neighbours for which $v_{i,j,k}^{p,q,r} < 0$ and $N_1^{out}(i, j, k)$ are indexes of neighbours for which $v_{i,j,k}^{p,q,r} > 0$. Then, Eq. (80) becomes

$$\sum_{(p,q,r)\in N_1^{in}(i,j,k)} (T_{i+p,j+q,k+r}$$
$$+\nabla T_{i+p,j+q,k+r} \cdot (x_{i,j,k}^{p,q,r} - x_{i+p,j+q,k+r}))v_{i,j,k}^{p,q,r}$$
$$+\sum_{(p,q,r)\in N_1^{out}(i,j,k)} (T_{i,j,k}$$
$$+\nabla T_{i,j,k} \cdot (x_{i,j,k}^{p,q,r} - x_{i,j,k}))v_{i,j,k}^{p,q,r}$$
$$-\sum_{(p,q,r)\in N_1^{in}(i,j,k)} T_{i,j,k}v_{i,j,k}^{p,q,r}$$
$$-\sum_{(p,q,r)\in N_1^{out}(i,j,k)} T_{i,j,k}v_{i,j,k}^{p,q,r} = |V_{i,j,k}|g, \qquad (82)$$

where $v_{i,j,k}^{p,q,r}$ is approximated by

$$v_{i,j,k}^{p,q,r} = |e_{i,j,k}^{p,q,r}|(v \cdot \mathbf{n}_{i,j,k}^{p,q,r}), \qquad (83)$$

where $|e_{i,j,k}^{p,q,r}|$ is the area of the face $e_{i,j,k}^{p,q,r}$. By using the functions $\max(0, v_{i,j,k}^{p,q,r})$ and $\min(0, v_{i,j,k}^{p,q,r})$, we can write

$$\sum_{(p,q,r)\in N_1} \Big[(T_{i+p,j+q,k+r}$$
$$+\nabla T_{i+p,j+q,k+r} \cdot (x_{i,j,k}^{p,q,r} - x_{i+p,j+q,k+r})) \min(0, v_{i,j,k}^{p,q,r})$$
$$+(T_{i,j,k} + \nabla T_{i,j,k} \cdot (x_{i,j,k}^{p,q,r} - x_{i,j,k})) \max(0, v_{i,j,k}^{p,q,r})$$
$$-T_{i,j,k}v_{i,j,k}^{p,q,r}\Big] = |V_{i,j,k}|g. \qquad (84)$$

The gradient on the finite volume $V_{i,j,k}$ can be expressed using derivatives in three linear independent directions. Let us denote these directions $\mathbf{p}, \mathbf{q}, \mathbf{r}$. For derivatives in these directions apply

$$\frac{\partial T}{\partial \mathbf{p}} = \nabla T \cdot \mathbf{p} = \frac{\partial T}{\partial x}p_x + \frac{\partial T}{\partial y}p_y + \frac{\partial T}{\partial z}p_z,$$
$$\frac{\partial T}{\partial \mathbf{q}} = \nabla T \cdot \mathbf{q} = \frac{\partial T}{\partial x}q_x + \frac{\partial T}{\partial y}q_y + \frac{\partial T}{\partial z}q_z,$$
$$\frac{\partial T}{\partial \mathbf{r}} = \nabla T \cdot \mathbf{r} = \frac{\partial T}{\partial x}r_x + \frac{\partial T}{\partial y}r_y + \frac{\partial T}{\partial z}r_z. \qquad (85)$$

If we look at (85) as a system of linear equations for unknowns $\frac{\partial T}{\partial x}, \frac{\partial T}{\partial y}, \frac{\partial T}{\partial z}$, we obtain the solution

$$\frac{\partial T}{\partial x} = -\frac{-p_z q_y \frac{\partial T}{\partial \mathbf{r}} + p_y q_z \frac{\partial T}{\partial \mathbf{r}} - q_z \frac{\partial T}{\partial \mathbf{p}}r_y + p_z \frac{\partial T}{\partial \mathbf{q}}r_y + q_y \frac{\partial T}{\partial \mathbf{p}}r_z - p_y \frac{\partial T}{\partial \mathbf{q}}r_z}{p_z q_y r_x - p_y q_z r_x - p_z q_x r_y + p_x q_z r_y + p_y q_x r_z - p_x q_y r_z},$$
$$\frac{\partial T}{\partial y} = -\frac{p_z q_x \frac{\partial T}{\partial \mathbf{r}} - p_x q_z \frac{\partial T}{\partial \mathbf{r}} + q_z \frac{\partial T}{\partial \mathbf{p}}r_x - p_z \frac{\partial T}{\partial \mathbf{q}}r_x - q_x \frac{\partial T}{\partial \mathbf{p}}r_z + p_x \frac{\partial T}{\partial \mathbf{q}}r_z}{p_z q_y r_x - p_y q_z r_x - p_z q_x r_y + p_x q_z r_y + p_y q_x r_z - p_x q_y r_z},$$
$$\frac{\partial T}{\partial z} = -\frac{-p_y q_x \frac{\partial T}{\partial \mathbf{r}} + p_x q_y \frac{\partial T}{\partial \mathbf{r}} - q_y \frac{\partial T}{\partial \mathbf{p}}r_x + p_y \frac{\partial T}{\partial \mathbf{q}}r_x + q_x \frac{\partial T}{\partial \mathbf{p}}r_y - p_x \frac{\partial T}{\partial \mathbf{q}}r_y}{p_z q_y r_x - p_y q_z r_x - p_z q_x r_y + p_x q_z r_y + p_y q_x r_z - p_x q_y r_z}, \qquad (86)$$

and thus

$$\nabla T_{i,j,k} = \frac{\mathbf{p} \times \mathbf{q}\frac{\partial T}{\partial \mathbf{r}} + \mathbf{q} \times \mathbf{r}\frac{\partial T}{\partial \mathbf{p}} + \mathbf{r} \times \mathbf{p}\frac{\partial T}{\partial \mathbf{q}}}{\det(\mathbf{p}, \mathbf{q}, \mathbf{r})}, \qquad (87)$$

where

$$\det(\mathbf{p}, \mathbf{q}, \mathbf{r}) = \det \begin{pmatrix} p_x & p_y & p_z \\ q_x & q_y & q_z \\ r_x & r_y & r_z \end{pmatrix}. \tag{88}$$

If the finite volume, on which we want to reconstruct the gradient, is the inner finite volume, $\mathbf{p}, \mathbf{q}, \mathbf{r}$ are defined by

$$\mathbf{p} = \frac{\mathbf{x}_{i+1,j,k} - \mathbf{x}_{i-1,j,k}}{|\mathbf{x}_{i+1,j,k} - \mathbf{x}_{i-1,j,k}|},$$
$$\mathbf{q} = \frac{\mathbf{x}_{i,j+1,k} - \mathbf{x}_{i,j-1,k}}{|\mathbf{x}_{i,j+1,k} - \mathbf{x}_{i,j-1,k}|},$$
$$\mathbf{r} = \frac{\mathbf{x}_{i,j,k+1} - \mathbf{x}_{i,j,k-1}}{|\mathbf{x}_{i,j,k+1} - \mathbf{x}_{i,j,k-1}|}. \tag{89}$$

Approximation of derivatives in these directions is

$$\frac{\partial T}{\partial \mathbf{p}} \approx \frac{T_{i+1,j,k} - T_{i-1,j,k}}{|\mathbf{x}_{i+1,j,k} - \mathbf{x}_{i-1,j,k}|},$$
$$\frac{\partial T}{\partial \mathbf{q}} \approx \frac{T_{i,j+1,k} - T_{i,j-1,k}}{|\mathbf{x}_{i,j+1,k} - \mathbf{x}_{i,j-1,k}|},$$
$$\frac{\partial T}{\partial \mathbf{r}} \approx \frac{T_{i,j,k+1} - T_{i,j,k-1}}{|\mathbf{x}_{i,j,k+1} - \mathbf{x}_{i,j,k-1}|}, \tag{90}$$

On the other hand, if the finite volume is the boundary finite volume, then one of the neighbouring finite volumes does not exist. Let us say finite volume $V_{i-1,j,k}$ does not exist. Then, we cannot use $T_{i-1,j,k}$ for reconstruction, but we can use the oblique derivative $g(\mathbf{x}_{ijk})$ in direction $\mathbf{v}(\mathbf{x}_{ijk})$. Let us denote them g and $\mathbf{v}$. Then, $\mathbf{p}, \mathbf{q}, \mathbf{r}$ are defined by

$$\mathbf{p} = \mathbf{v},$$
$$\mathbf{q} = \frac{\mathbf{x}_{i,j+1,k} - \mathbf{x}_{i,j-1,k}}{|\mathbf{x}_{i,j+1,k} - \mathbf{x}_{i,j-1,k}|},$$
$$\mathbf{r} = \frac{\mathbf{x}_{i,j,k+1} - \mathbf{x}_{i,j,k-1}}{|\mathbf{x}_{i,j,k+1} - \mathbf{x}_{i,j,k-1}|}. \tag{91}$$

Approximation of derivatives in these directions is

$$\frac{\partial T}{\partial \mathbf{p}} = g,$$
$$\frac{\partial T}{\partial \mathbf{q}} \approx \frac{T_{i,j+1,k} - T_{i,j-1,k}}{|\mathbf{x}_{i,j+1,k} - \mathbf{x}_{i,j-1,k}|},$$
$$\frac{\partial T}{\partial \mathbf{r}} \approx \frac{T_{i,j,k+1} - T_{i,j,k-1}}{|\mathbf{x}_{i,j,k+1} - \mathbf{x}_{i,j,k-1}|}, \tag{92}$$

And so

$$\nabla T_{i,j,k}$$
$$= \frac{\mathbf{v} \times \mathbf{q} \, \dfrac{T_{i,j,k+1} - T_{i,j,k-1}}{|x_{i,j,k+1} - x_{i,j,k-1}|} + \mathbf{q} \times \mathbf{r}\, g + \mathbf{r} \times \mathbf{v} \, \dfrac{T_{i,j+1,k} - T_{i,j-1,k}}{|x_{i,j+1,k} - x_{i,j-1,k}|}}{\det(\mathbf{v}, \mathbf{q}, \mathbf{r})}. \tag{93}$$

Substituting (93) into the (84), we get equations for boundary finite volumes $V_{i,j,k} \in O$. Due to the construction of our scheme, the equations for these finite volumes may require two neighbouring finite volumes in the directions of $\mathbf{q}$ and $\mathbf{r}$. For those which do not have such neighbours, we have to prescribe Dirichlet boundary conditions, which is also in accordance with the compatibility of boundary conditions mentioned in the introduction. All these equations together with equations from the discretization of the Laplace equation form a numerical scheme for solving the problem (1).

4 Numerical experiments

In this section, we present numerical experiments for the geodetic BVP (1–3). An experimental order of convergence is studied in the first two experiments. Next experiments present a reconstruction of a harmonic function on and above the complicated Earth's topography, namely over the Himalayas and in the area of Slovakia. This harmonic function as well as all boundary conditions (BCs) is generated from the global geopotential models that are based on the SH-based approach. The last experiment presents local gravity field modelling in Slovakia using terrestrial gravity data.

4.1 Experimental order of convergence

In the first experiment, we are solving the BVP (1–3) with BCs obtained from an artificial harmonic function defined on a computational domain, see Fig. 6. This computational domain is bounded by four planar side boundaries, a spherical upper boundary and the bottom boundary, which is given by a perturbed sphere. In order to test the numerical scheme, we constructed the most coarse grid using the method presented in Sect. 2. Then, refined grids were constructed by adding new representative points in between representative points of the previous grid using Eq. (60). The exact solution was chosen as $T(\mathbf{x}) = \frac{1}{|\mathbf{x} - (0.1, 0.2, 0.3)|}$, and its values were used to generate the oblique derivative and the Dirichlet BC. The oblique derivative BC was prescribed on the perturbed sphere as the bottom boundary. The vectors in the direction of $\nabla T(\mathbf{x})$ were rotated alternately by the angle of $\pi/6$ around x, y, z axes to get the vectors v, see Fig. 7. Then, the FVM presented in Sect. 3 was used to solve this problem. Table 1 depicts the L_2-norm and maximum norm of residuals
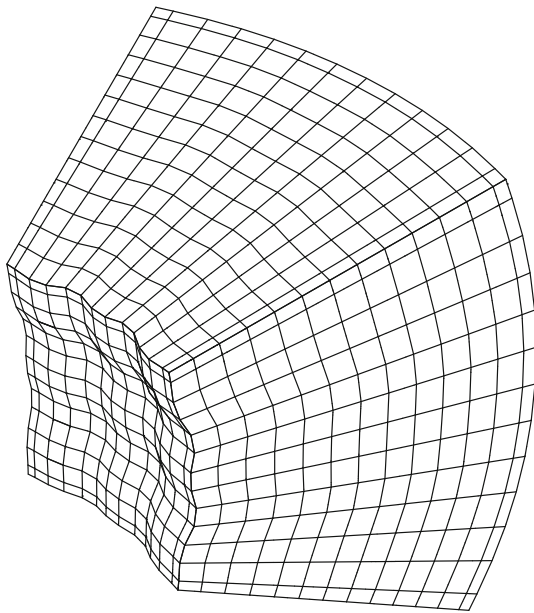
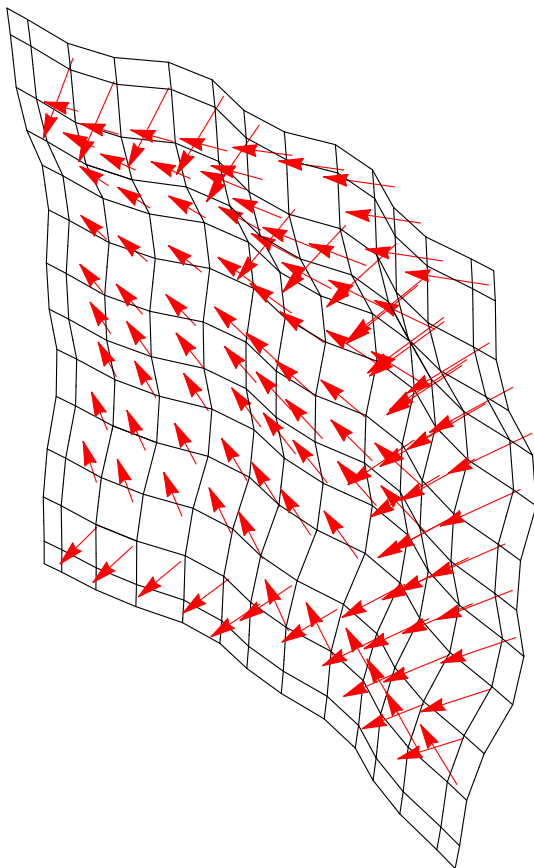**Fig. 6** Computational domain for the first experiment

Fig. 7 Oblique derivative directions for the first experiment

Table 1 L_2 norm and *max* norm of residuals, and EOC of FVM for the problem with the exact solution $T(\mathbf{x}) = |\mathbf{x} - (0.1, 0.2, 0.3)|^{-1}$

$h_{\max}$	$||e_{h_{\max}}||_{L_2}$	EOC	$||e_{h_{\max}}||_{\max}$	$EOC_{\max}$
0.125	0.000229		0.00269	
0.0642	7.00358e−05	1.761	0.00102	1.429
0.0324	2.43723e−05	1.545	0.000418	1.31582
0.0162	7.90755e−06	1.635	0.000153	1.45607
0.00817	2.44251e−06	1.702	5.23081e−05	1.56279

The EOC is defined as follows. Let us assume that the error of the scheme in some norm is proportional to some power of the grid size, i.e. $||e_h|| = Ch^\alpha$, with a constant C. The error of the scheme e_h is defined as a difference between the exact and numerical solutions. Then, having two grids with the maximal diameter of the finite volumes $h_{\max_1}$ and $h_{\max_2}$, where $h_{\max_1} > h_{\max_2}$, we can obtain numerically two errors $||e_{h_{\max_1}}|| = Ch^\alpha_{\max_1}$ and $||e_{h_{\max_2}}|| = Ch^\alpha_{\max_2}$. We can see that

$$\frac{||e_{h_{\max_1}}||}{||e_{h_{\max_2}}||} = \frac{Ch^\alpha_{\max_1}}{Ch^\alpha_{\max_2}} = \left(\frac{h_{\max_1}}{h_{\max_2}}\right)^\alpha \quad (94)$$

from where we can simply extract

$$\alpha = \log_{\frac{h_{\max_1}}{h_{\max_2}}} \frac{||e_{h_{\max_1}}||}{||e_{h_{\max_2}}||}, \quad (95)$$

which is called the experimental order of convergence (EOC) of the scheme. We will use the numerical L_2 norm for evaluating the EOC.

The second experiment is computed on the same computational domain with the exact solution taken from EGM2008 while using only the SH coefficients up to degree and order 5. The oblique derivative is generated as the first derivative of the disturbing potential (the exact solution) in the radial direction. This radial direction represents the oblique direction since it differs from the direction of the normal vector to the bottom boundary. Table 2 shows the L_2-norm and maximum norm of residuals between the obtained FVM solutions and exact solution, and the achieved EOC. Both experiments show that EOC of our FVM approach is about 1.6, which means that if we decrease the maximal size of the finite volumes by 2, then the error of our solution will decrease approximately by 3 ($2^{1.6} \approx 3.03$).

4.2 Reconstruction of EGM2008 over the Himalayas

Next experiments aim to demonstrate the decreasing error of our FVM solution with refining the computational grid above the extremely complicated Earth's topography in the

between the obtained FVM solutions and the exact solution, and the achieved experimental order of convergence (EOC) of our FVM approach.

Table 2 L_2 norm and *max* norm of residuals, and EOC of FVM for the problem with exact solution taken from the EGM2008 up to degree and order 5

h_{max}	$\|e_{h_{max}}\|_{L_2}$	EOC	$\|e_{h_{max}}\|_{max}$	EOC_{max}
0.125	9.25506e−05		0.000911	
0.0642	2.39154e−05	2.01	0.000348	1.43
0.0324	8.80662e−06	1.462	0.0001389	1.349
0.0162	2.96979e−06	1.579	4.87918e−05	1.51659
0.00817	9.39478e−07	1.667	1.5969e−05	1.61833

Himalayas. The EGM2008 up to degree 2160 was used to generate all BCs and the harmonic function.

These numerical experiments were performed in the domain above the Himalayas bounded by $\langle 60°, 110° \rangle$ meridians and $\langle 20°, 50° \rangle$ parallels. The 3D computational grid was generated using method described in Sect. 2. The bottom boundary was given by grid points that are located on the Earth's surface. Their spacing in horizontal directions was uniform. Their heights were interpolated from the SRTM30 PLUS topography model (Becker et al. 2009), see Fig. 8a. An
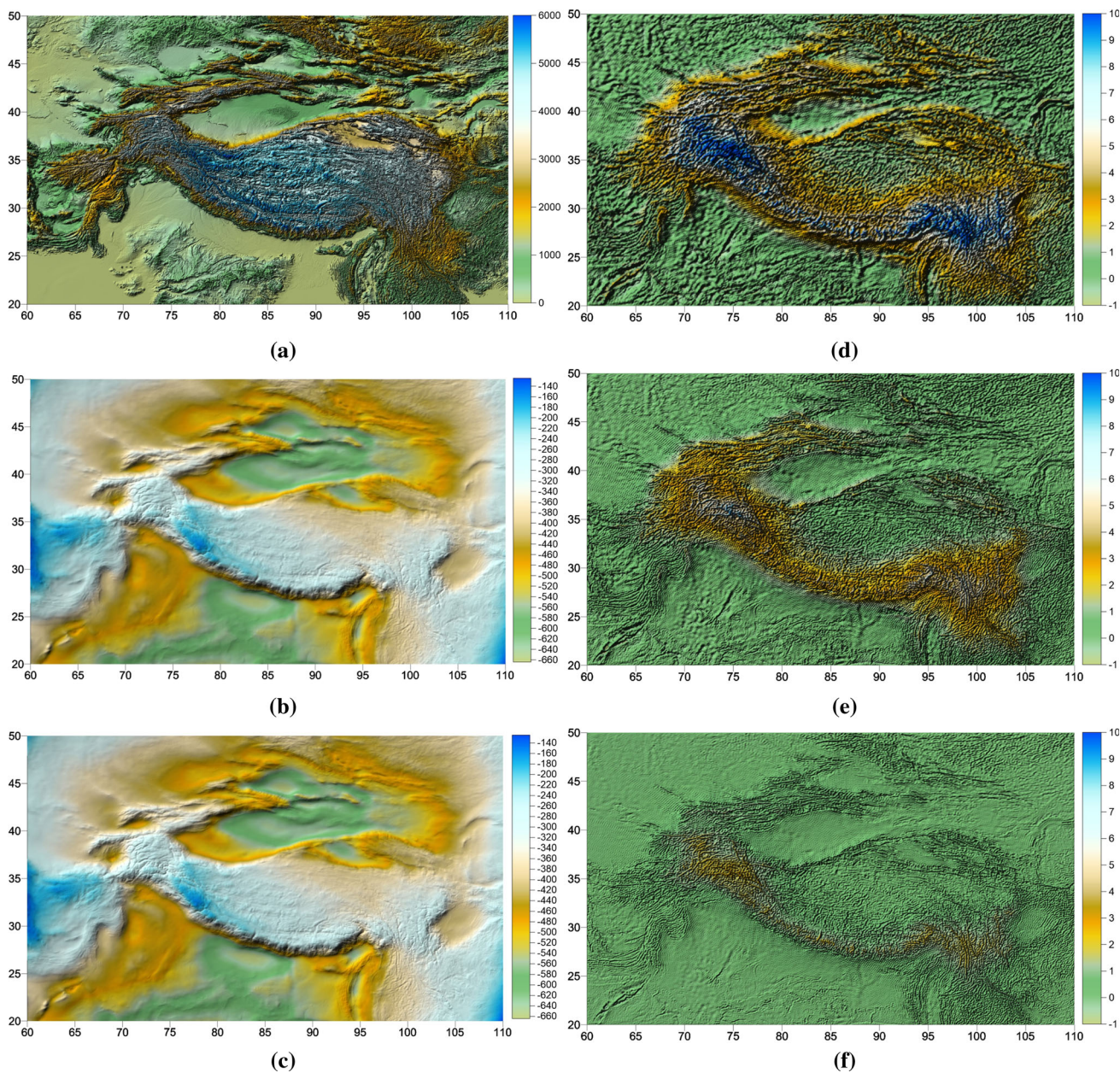
Fig. 8 **a** Earth's surface topography over the Himalayas (the bottom boundary) (m), **b** the disturbing potential from EGM2008 on the Earth's surface $(m^2 s^{-2})$, **c** the disturbing potential from our FVM solution $(m^2 s^{-2})$, (**d**, **e**, **f**) residuals between the EGM2008 and our FVM solution, where grid density is **d** $501 \times 301 \times 25$, **e** $1001 \times 601 \times 49$, **f** $2001 \times 1201 \times 97$ points $(m^2 s^{-2})$

Table 3 Statistics of residuals between our FVM solution and the EGM2008 in the domain above the Himalayas ($m^2 s^{-2}$)

Resolution grid density	$0.1° \times 0.1° \times 10$ km $501 \times 301 \times 25$	$0.05° \times 0.05° \times 5$ km $1001 \times 601 \times 49$	$0.025° \times 0.025° \times 2.5$ km $2001 \times 1201 \times 97$
Min. value	−5.07	−1.68	−0.44
Mean value	1.79	0.87	0.33
Max. value	23.05	11.98	3.90
St. deviation	2.3	1.09	0.37

upper boundary was chosen in the height of 240 *km* above a reference ellipsoid corresponding to an average altitude of the GOCE satellite orbits. The resulting 3D computational grid constructed by our surface evolution method (see Sect. 2) is non-uniform. On the bottom boundary, the first derivatives in the radial direction were prescribed that represented the oblique derivative BC. On the rest of the boundary, the Dirichlet BC in form of the disturbing potential was prescribed. All these BCs were generated from the EGM2008 model up to degree 2160.

Three experiments with different grid densities were performed, namely the grids with the densities $501 \times 301 \times 25$, $1001 \times 601 \times 49$ and $2001 \times 1201 \times 97$ points. They approximately correspond to spacing $0.1° \times 0.1° \times 10$ km, $0.05° \times 0.05° \times 5$ km and $0.025° \times 0.025° \times 2.5$ km.

Figure 8b shows EGM2008 at points on the Earth's topography as the harmonic function that we are reconstructing. The obtained FVM solution for the most dense grid is depicted in Fig. 8c. Residuals between EGM2008 and our FVM solutions on the bottom boundary are shown in Fig. 8c–e. The statistical characteristics of the corresponding residuals are summarized in Table 3. It is evident that refinements of the grid lead to higher accuracy of the FVM solution giving better agreement with EGM2008. Standard deviations (STDs) are decreasing from 2.3 to 0.37 $m^2 s^{-2}$ ($\sim$ 2.3 dm to 3.7 cm) and the maximal values from 23.1 to 3.9 $m^2 s^{-2}$ ($\sim$ from 2.3 m to 3.9 dm). Such an improvement is achieved despite the fact that refinements of the grids involve more detailed consideration of the topography. This confirms efficiency of our approach.

4.3 Reconstruction of EIGEN-6C4 over Slovakia

The next local numerical experiment is similar to the previous one, but it was performed in the domain above Slovakia and the EIGEN-6C4 model up to degree 2160 (Förste et al. 2014) was used to generate all BCs and the harmonic function. The domain was bounded by ⟨16°, 24°⟩ meridians and ⟨47°, 50°⟩ parallels. Due to the smaller area of the computational domain, the grid density is higher in this experiment; namely, the resolution is $0.008° \times 0.008° \times 600$ m. The upper boundary is at the same height of 240 km above the reference ellipsoid. The heights of grid points on the bottom boundary were interpolated from SRTM30 PLUS model, see Fig. 9a.

Here the first derivatives in the radial direction were prescribed. On the rest of the boundary, the Dirichlet BCs in the form of the disturbing potential were prescribed. All the BCs were generated from the EIGEN-6C4 model up to degree 2160.

An experiment with the density $1001 \times 376 \times 401$ was performed using the FVM approach. The disturbing potential on the Earth's topography generated from EIGEN-6C4 is depicted in Fig. 9b. The obtained FVM solution was compared with EIGEN-6C4, see Fig. 9c. The statistical characteristics of the residuals on the bottom boundary are summarized in Table 4. High value of residuals, reaching up to 0.25 $m^2 s^{-2}$ ($\sim$ 2.6 cm), are located in the area of Tatra mountains (the north part of central Slovakia) most likely due the complicated topography. Here further grid refinements should be applied to achieve better results. However, in the rest of the domain the residuals are below 0.1 $m^2 s^{-2}$ ($\sim$ 1 cm). The STD of all residuals is 0.022 $m^2 s^{-2}$ ($\sim$ 2.2 mm). It confirms high accuracy of the presented method taking into account that we solve the geodetic BVP on the non-uniform grids above the very detailed Earth's topography.

4.4 Local gravity field modelling over Slovakia from terrestrial gravity data

Finally, we present local gravity field modelling over Slovakia using terrestrial gravity data. The goal of this experiment is to compare efficiency of our new FVM scheme with the previous ones developed on uniform grids, namely with the central scheme (Macák et al. 2014) and an upwind scheme (Macák et al. 2015). For these purposes, we used the same sources of input data yielding the same BCs as in the numerical experiments presented in those papers. Namely, on the upper and side boundaries, the GOCO03S model up to degree 250 (Mayer-Gurr et al. 2012) was used to generate the Dirichlet BCs. On the bottom boundary, we used the surface gravity disturbances obtained from the available regular grid of gravity anomalies, with the resolution $20'' \times 30''$, that was compiled from original gravimetric measurements (Grand et al. 2001). To transform these gravity anomalies into the gravity disturbances, we used the official digital vertical reference model—DVRM (www.geoportal.sk). The grid density in this experiment was adopted from the source

Fig. 9 a Earth's surface topography over Slovakia, **b** the disturbing potential on the Earth's surface generated from EIGEN-6C4 (m^{2}s^{-2}), **c** residuals between EIGEN-6C4 and our FVM solution (m^{2}s^{-2})

(a)

(b)

(c)
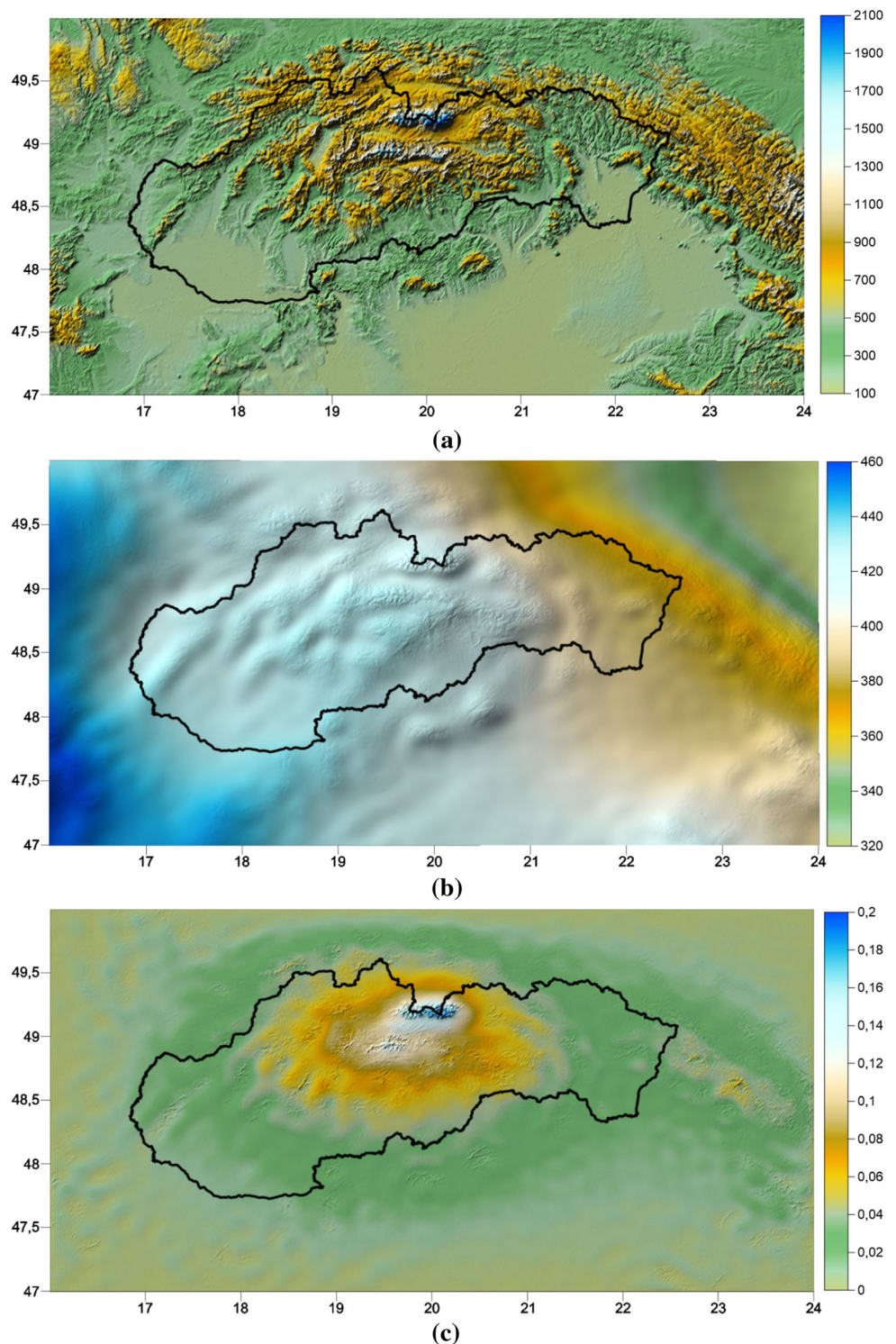
dataset and was the same as in the aforementioned papers, namely $20'' \times 30'' (\Delta\varphi \times \Delta\lambda)$. The only difference was that in our case such surface gravity disturbances were considered on the Earth's topography.

The domain was bounded by $\langle 16°, 23° \rangle$ meridians and $\langle 47°, 50.5° \rangle$ parallels. Similarly as in the experiments of the aforementioned papers, the side boundaries were chosen sufficiently far from the area of Slovakia in order to mitigate an influence of the prescribed Dirichlet BC generated from the satellite-only geopotential model. For more details about this influence, see Fašková et al. (2010). The heights were inter-

Table 4 Statistics of residuals between our FVM solution and EIGEN-6C4 (m^2s^{-2})

Min. value	0.011
Mean value	0.021
Max. value	0.26
St. deviation	0.022

polated from SRTM30 PLUS model and the upper boundary is again in the height of 240 km above the reference ellipsoid.

An experiment with the density $841 \times 631 \times 301$ was performed using the FVM approach. The obtained disturbing potential on the Earth's surface was transformed to the local quasigeoid model of Slovakia. Its quality was tested using GNSS-levelling. From the available dataset of 61 GNSS-levelling benchmarks, three evident outliers were removed. Hence, we tested the obtained local quasigeoid model as well as the previous FVM-based models and EGM2008 at 58 points (Fig. 10).

Table 5 presents the statistical characteristics of the residuals. They indicate that our FVM approach on non-uniform grids gives better results than the previous FVM solutions considered on uniform grids. Using our new FVM scheme, we were able to reduce the standard deviation by 3 mm and the range by 2.2 cm compared to the upwind scheme on

a uniform grid (Macák et al. 2015). Although EGM2008 outperforms our FVM local quasigeoid model in terms of STD by 6 mm, the range of residuals decreases by 6.1 cm. Nevertheless, we hope that a further refinement of the computational grid will lead to more precise FVM solutions. An obvious advantage of our approach is that the FVM solution is obtained at points directly on the Earth's topography.

5 Discussion and conclusions

In this paper, we have presented an original numerical method for solving the oblique derivative boundary value problem. Namely, the finite volume method on non-uniform grids above the Earth's topography has been developed, in which the oblique derivative boundary condition has been treated as a stationary advection equation. A new method for discretization of the computational domain has been proposed that is based on an evolution of the Earth's surface depending on its mean curvature. It involves a tangential redistribution of the evolving surface discretization points leading to a construction of a more regular non-uniform 3D hexahedron grid. Then, we have introduced a discretization of the Laplace equation and oblique derivative boundary condition
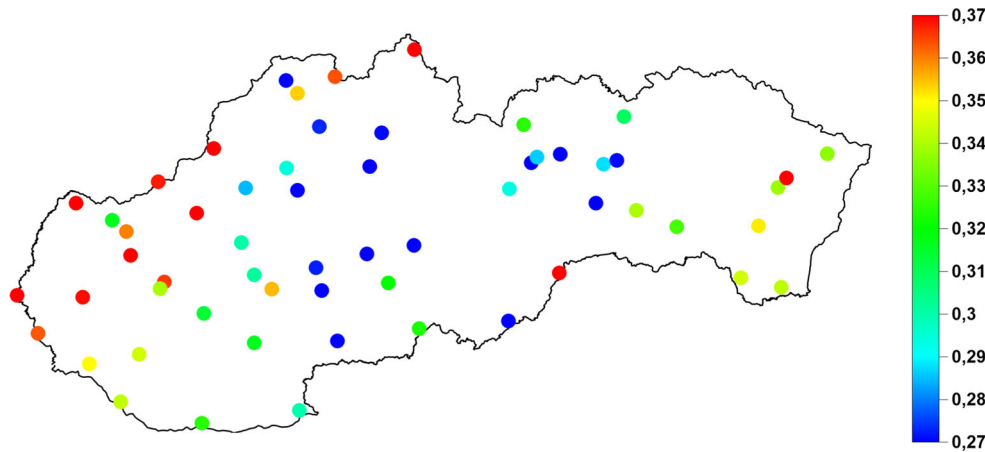
Fig. 10 GNSS-leveling test (m) at 58 points in area of Slovakia-set of points used for testing are visualised

Table 5 GNSS-leveling test (m) at 58 points in area of Slovakia

	EGM2008	FVM			
		Neum. BC*	Oblique derivative BC		
			Central sch.*	Upwind sch.** uniform grid	Upwind sch. non-uniform grid
Min value	0.301	0.104	0.168	0.173	0.227
Mean value	0.437	0.236	0.277	0.282	0.323
Max value	0.584	0.393	0.419	0.417	0.450
Range	0.283	0.288	0.251	0.244	0.222
STD	0.044	0.068	0.054	0.053	0.050

*Results published in Macák et al. (2014), **results published in Macák et al. (2015)

on such non-uniform grids. It consists of a reconstruction of the normal derivative to the finite volume using derivatives in the tangential directions. To treat numerically the oblique derivative BC as an advection equation, a new higher-order upwind method has been introduced for non-uniform grids.

The presented numerical experiments have aimed to demonstrate efficiency of our proposed numerical method. The first experiments have confirmed that the numerical discretization converges to the exact solutions when refining the grid with the experimental order of convergence equal approximately to 1.6. This indicates an apparent improvement when comparing with the previous scheme derived and tested on the uniform grids, where the experimental order of convergence was about 1.0 (Macák et al. 2015).

The next numerical experiment, dealing with the reconstruction of EGM2008 as a harmonic function, has shown that the proposed numerical method converges to the exact solution also on extremely complicated computational domains, namely above the Himalayas. However, the convergence of the chosen BiCGStab linear solver has been slow in this case, which can be caused by complicated shapes of the non-uniform 3D hexahedron grids in the neighbourhood of such extremely mountainous topography. To improve such slower convergence, some efficient preconditioning should be implemented into the linear solver.

The last numerical experiment has been dealing with the local gravity field modelling over Slovakia using terrestrial gravity data. The GNSS-levelling test has shown an improvement in the standard deviation and range of residuals when comparing with the previous FVM numerical schemes. This test has indicated that the new upwind scheme has approximated the oblique derivative BC more accurately than the central scheme (Macák et al. 2014) or the first-order upwind scheme on uniform grids (Macák et al. 2015) while the same level of discretization has been considered. Based on these achieved results, we expect that a further refinement of the computational grid could lead to even more accurate results. For this goal, a parallelization using the MPI procedures as well as efficient preconditioning should be implemented.

Finally, it is worth to note that the developed method for discretization of the computational domain into non-uniform grids can be useful for other applications in geosciences as well. It may provide an important basis for solving numerically various geoscientific problems described by partial differential equations.

References

Bauer F (2004) An alternative approach to the oblique derivative problem in potential theory. PhD thesis, Geomathematics Group, Department of Mathematics, University of Kaiserslautern. Shaker Verlag, Aachen, Germany

Becker JJ, Sandwell DT, Smith WHF, Braud J, Binder B, Depner J, Fabre D, Factor J, Ingalls S, Kim SH, Ladner R, Marks K, Nelson S, Pharaoh A, Trimmer R, Von Rosenberg J, Wallace G, Weatherall P (2009) Global Bathymetry and elevation data at 30 arc seconds resolution: SRTM30 PLUS. Mar Geod 32(4):355–371

Bitzadse AV (1968) Boundary-value problems for second-order elliptic equations. North-Holland, Amsterdam

Bjerhammar A, Svensson L (1983) On the geodetic boundary value problem for a fixed boundary surface. A satellite approach. Bull Geod 57(1–4):382–393

Bruinsma SL, Frste C, Abrikosov O, Lemoine J-M, Marty J-C, Mulet S, Rio M-H, Bonvalot S (2014) ESA's satellite-only gravity field model via the direct approach based on all GOCE data. Geophys Res Lett 41(21):7508–7514

Čunderlík R, Mikula K (2010) Direct BEM for high-resolution gravity field modelling. Stud Geophys Geod 54(2):219–238

Čunderlík R, Mikula K, Mojžeš M (2008) Numerical solution of the linearized fixed gravimetric boundary-value problem. J Geod 82:15–29

Čunderlík R, Mikula K, Špir R (2012) An oblique derivative in the direct BEM formulation of the fixed gravimetric BVP. IAG Symp 137:227–231

Fašková Z (2008) Numerical methods for solving geodetic boundary value problems. PhD thesis, SvF STU, Bratislava, Slovakia

Fašková Z, Čunderlík R, Mikula K (2010) Finite element method for solving geodetic boundary value problems. J Geod 84(2):135–144

Förste Ch, Bruinsma SL, Abrikosov O, Lemoine J-M, Marty JC, Flechtner F, Balmino G, Barthelmes F, Biancale R (2014) EIGEN-6C4 The latest combined global gravity field model including GOCE data up to degree and order 2190 of GFZ Potsdam and GRGS Toulouse. GFZ Data Serv. doi:10.5880/icgem.2015.1

Freeden W (1987) Harmonic splines for solving boundary value problems of potential theory. In: Mason JC, Cox MG (eds) Algorithms for approximation, the institute of mathematics and its applications, conference series, vol 10. Clarendon Press, Oxford, pp 507–529

Freeden W, Gerhards C (2013) Geomathematically oriented potential theory. CRC Press, Boca Raton

Freeden W, Kersten H (1980) The geodetic boundary value problem using the known surface of the earth. Veroff Geod Inst RWTH Aachen, no. 29

Freeden W, Kersten H (1981) A constructive approximation theorem for the oblique derivative problem in potential theory. Math Methods Appl Sci 3:104–114

Freeden W, Michel V (2004) Multiscale potential theory (with applications to geoscience). Birkhuser, Boston

Grand T, Šefara J, Pašteka R, Bielik M, Daniel S (2001) Atlas of geophysical maps and profiles, part D1: gravimetry. Final report, State Geological Institute, Bratislava, MS Geofond (in Slovak)

Grothaus M, Raskop T (2009) The outer oblique boundary problem of potential theory. Numer Funct Anal Optim 30:711–750

Gutting M (2007) Fast multipole methods for oblique derivative problems. PhD thesis, Geomathematics Group, Department of Mathematics, University of Kaiserslautern. Shaker Verlag, Aachen, Germany

Gutting M (2012) Fast multipole accelerated solution of the oblique derivative boundary value problem. Int J Geomath 3:223–252

Gutting M (2015) Fast spherical/harmonic spline modeling. In: Freeden W, Nashed M. Z, Sonar T (eds) Handbook of geomathematics, 2nd edn. Springer, Heidelberg, pp 2711–2746

Holota P (1997) Coerciveness of the linear gravimetric boundary-value problem and a geometrical interpretation. J Geod 71:640–651

Holota P, Nesvadba O (2008) Model refinements and numerical solution of weakly formulated boundary-value problems in physical geodesy. IAG Symp 132:320–326

Húska M, Medĺa M, Mikula K, Novysedlák P, Remešíková M (2012) A new form-finding method based on mean curvature flow of surfaces. In: Handlovičová A, Minárechová Z, Ševčovič) D (eds) ALGORITMY 2012, 19th conference on scientific computing, Podbanske, Slovakia, September 9–14, 2012, proceedings of contributed papers and posters. Publishing House of STU, pp 120–131. ISBN 978-80-227-3742-5

Klees R (1995) Boundary value problems and approximation of integral equations by finite elements. Manuscr Geod 20:345–361

Klees R, van Gelderen M, Lage C, Schwab C (2001) Fast numerical solution of the linearized Molodensky problem. J Geod 75:349–362

Koch KR, Pope AJ (1972) Uniqueness and existence for the geodetic boundary value problem using the known surface of the earth. Bull Geod 46:467–476

Lehmann R, Klees R (1999) Numerical solution of geodetic boundary value problems using a global reference field. J Geod 73:543–554

LeVeque RJ (2002) Finite Volume Methods for Hyperbolic Problems, Cambridge University Press, Cambridge, pp 525–531

Macák M (2014) Numerical methods in geodesy, PhD thesis, Faculty of Civil Engineering, Slovak University of Technology Bratislava. (in Slovak)

Macák M, Mikula K, Minárechová Z (2012) Solving the oblique derivative boundary-value problem by the finite volume method. In: ALGORITMY 2012, 19th conference on scientific computing, Podbanske, Slovakia, September 9–14, 2012, proceedings of contributed papers and posters, Publishing House of STU, pp 75–84

Macák M, Minarechová Z, Mikula K (2014) A novel scheme for solving the oblique derivative boundary-value problem. Stud Geophys Geo 58(4):556–570

Macák M, Čunderlík R, Mikula K, Minarechová Z (2015) An upwind-based scheme for solving the oblique derivative boundary-value problem related to the physical geodesy. J Geod Sci 5(1):180–188

Macák M, Mikula K, Minarechová Z, Čunderlík R (2016) On an iterative approach to solving the nonlinear satellite-fixed geodetic boundary-value problem. IAG Symp 142:185–192

Mayer-Gurr et al T (2012) The new combined satellite only model GOCO03s. Presented at the GGHS-2012 in Venice, Italy

Medĺa M (2012) Creating of the logically rectangular grids in 2D and 3D domains above the Earth topography, Bachelor thesis, Faculty of Civil Engineering, Slovak University of Technology Bratislava. (in Slovak)

Meissl P (1981) The use of finite elements in physical geodesy. Report 313, Geodetic Science and Surveying, The Ohio State University

Mikula K, Ševčovič D (2004) A direct method for solving an anisotropic mean curvature flow of planar curve with an external force. Math Methods Appl Sci 27(13):1545–1565

Mikula K, Remešiková M, Sarkóci P, Ševčovič D (2014) Manifold evolution with tangential redistribution of points. SIAM J Sci Comput 36(4):A1384–A1414

Minarechová Z, Macák M, Čunderlík R, Mikula K (2015) High-resolution global gravity field modelling by the finite volume method. Stud Geophys Geo 59:1–20

Miranda C (1970) Partial differential equations of elliptic type. Springer, Berlin

Nesvadba O, Holota P, Klees R (2007) A direct method and its numerical interpretation in the determination of the gravity field of the Earth from terrestrial data. IAG Symp 130:370–376

Pavlis NK, Holmes SA, Kenyon SC, Factor JK (2012) The development and evaluation of the Earth Gravitational Model 2008 (EGM2008). J Geophys Res 117:B04406. doi:10.1029/2011JB008916

Shaofeng B, Dingbo C (1991) The finite element method for the geodetic boundary value problem. Manuscr Geod 16:353–359

Sleijpen GLG, Fokkema DR (1993) Bicgstab (l) for linear equations involving unsymmetric matrices with complex spectrum. http://dspace.library.uu.nl/handle/1874/16827

Šprlák M, Fašková Z, Mikula K (2011) On the application of the coupled finite-infinite element method to the geodetic boundary value problem. Stud Geophys Geo 55:479–487